Beyond 5G White Paper
Supplementary Volume
“Cell-Free / Distributed MIMO ”

Version 1.0

March 7, 2024

Beyond 5G Promotion Consortium

White Paper Subcommittee

【Revision History】

Ver.	Date	Contents	Note
1.0	2024.3.7	Initial version	

Preface

The implementation of 5G mobile communication systems in society has been in full swing since around 2020. Mobile communication systems have become a social infrastructure that connects not only people but also things like the Internet of Things (IoT). A cyber-physical system (CPS) in which people interact with each other, people interact with things, and things interact with each other through cyberspace has come to have great significance in various aspects of social life. In the next-generation mobile communication system, it is expected that the communication network centered on the mobile communication system will function as the basic infrastructure of society in the future. Then, the evolution of the mobile communication systems continued to be required as the basic infrastructure for resolving various social issues, and to provide safe and prosperous living.

Cell-Free MIMO, also known as distributed MIMO, is one expected elemental technology to evolve the mobile communication systems drastically from various aspects by cooperating the distributed antennas. It has 2 major advantages for the evolution of the current system. One is to reduce the interference among the cells. As the growth of the mobile traffic, it has been required to increase system capacity and the cells densification have been required. But that increases interference at cell edge especially in the lower frequency band, and the communication quality would be more location dependent and it limits the service quality. The other is to keep a connection by utilizing multiple distributed antennas even under the severe radio propagation environment by shadowing and blockage as well as large pathloss, especially in the higher frequency band.

However, there still remains technical issues to realize and deploy it in reality. The major issues are as follows.

- To reduce complexity of the signal processing for improving scalability of the system when accommodating a large number of UEs in a large-scale network with massive number of distributed antennas.
- To increase fronthaul capacity or to reduce fronthaul load with realistic deployment cost and energy consumption.
- To provide wide coverage in a higher frequency band including sub-THz band with sophisticated and highly efficient beamforming technology at each antenna site.
- To enhance operation flexibility to satisfy diversified requirement of user's with keeping the total performance.
- To demonstrate the various concept of these technologies with testbed in a real environment.

Hence, research and development activities have been conducted actively in Japan, in telecom operators, network vendors, and academia from various aspects, and this white

paper introduces recent activities including results of demonstration trials and simulation results. Concretely, the following contents are introduced:

- Title1 Research activities towards wide area deployment of Cell-Free massive MIMO
- Title2 High-frequency Band Distributed Antenna System
- Title3 Real-Time Simulator for 6th Generation Mobile Communication System Using Distributed MIMO
- Title4 Distributed MIMO Technologies for High Frequency Bands
- Title5 Distributed Antenna Technology (High-density Distributed Antenna System, and Transmission Point Sharing Control
- Title6 User Cluster-centric Approach for Cell-free Massive MIMO Systems
- Title7 Low-Complexity User-Centric TRP Clustering Method in Downlink Cell-Free MIMO with Regularized ZF-Based Beamforming
- Title8 Toward Practical Cell-Free MIMO Network

This White Paper was prepared with the generous support of many people who participated in the White Paper Subcommittee. The cooperation of telecommunications industry players and academia experts, as well as representatives of various industries other than the communications industry has also been substantial. Thanks to everyone's participation and support, this White Paper was able to cover a lot of useful information for future business creation discussions between the industry, academia, and government, and for investigating solutions to social issues, not only in the telecommunications industry, but also across all industries. We hope that this White Paper will help Japan create a better future for society and promote significant global activities.

Issei Kanno KDDI Research Inc.

1 Research activities towards wide area deployment of Cell-Free massive MIMO

Issei Kanno KDDI Research Inc.
Noboru Osawa KDDI Research Inc.
Masaaki Ito KDDI Research Inc.
Hiroyuki Shinbo KDDI Research Inc.

Abstract—**This article introduces research activities for realizing cell-free massive MIMO especially for its large-scale deployment aiming to provide great wireless quality everywhere in a wide area. Concretely, the activities include: (1) user centric clustering to have scalability of the signal processing at a central site including its demonstration trial, (2) IFoF (IF over fiber) fronthaul technology to reduce deployment cost and to ensure installation easiness, (3) pilot decontamination scheme to enhance the capacity for increasing the number of spatial multiplexing, and (4) AP (access point) on/off switching technology for energy efficient operation.**

1.1 Introduction

Cell-Free massive MIMO is a promising technology for improving performance of wireless communication from various perspectives by distributing a large number of APs in an area and operating them cooperatively with signal processing at a central site, and it is regarded as one on the fundamental technologies for future communication systems such as 6G [1]. As a communication operator’ s perspective, it is expected to deploy service area with great wireless communication quality and provide communication services of various use cases including mission critical one everywhere in the area. In addition, it is also expected to reduce cost and workload for cell planning and maintenance of the service area because the interference among densified cells can be mitigated by the signal processing and autonomous coordination at the central site in this technology. A great deal of research has been conducted including the relevant technologies such as distributed MIMO and CoMP (Coordinated Multi-Point). However, in terms of its wide area deployment with distributing large number of antennas, there still remain various technical issues. This article introduces our several research activities for the issues.

1.2 User centric clustering for scalability and its demonstration trial

One critical issue for deploying large-scale cell-free massive MIMO is its scalability, which requires limiting computational complexity in order to operate on a large scale at the central site. In the large-scale network, accommodating many APs and UEs (user equipment), the computational complexity of the signal processing for precoding and multi-user detection grows prohibitively, which is not practical. To reduce the complexity

effectively, we have focused on user centric clustering and its signal processing, which limits the number of APs to process signals of each UE with reducing the interference to other UEs by the partial processing. For the operation, it is efficient and simple to select those APs which are located closely to each UE individually at each moment. This can be viewed as if the selected APs are operated to customize the service area for the UE at each moment, and that is called as user centric clustering. To demonstrate this concept, we have developed a testbed and conducted a field trial [2]. In the trail, the testbed is operated with 8 APs at 4.5GHz frequency band, and 4 UEs are spatially multiplexed in downlink by utilizing the user centric clustering and partial MMSE precoding. The results show that those schemes are operated successfully, and each UE can obtain better throughput everywhere in a target area compared to cellular operation mode, where each AP is operated independently for a UE. Note that the throughput corresponds to that of one UE that is moving along the grids, where the rest 3 UEs are located in a fixed position.

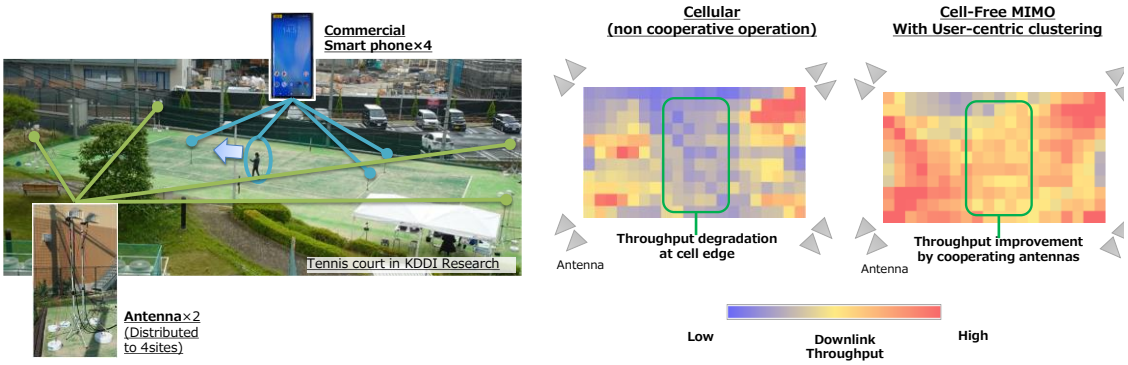

Fig. 1-1 Demonstration trial of cell-free massive MIMO with user centric clustering

1.3 IFoF based mobile fronthaul for cell-free massive MIMO

Another critical issue for the large-scale cell-free massive MIMO is to deploy the fronthaul in a realistic cost whereas its required capacity and link further increases.. Recently, ARoF (Analog RoF), which achieves large capacity by converting analog RF waveform to the optical signal, has been attracted much attention of its applicability to further wideband transmission targeting 6G. It is noteworthy that such ARoF schemes do not require ADC/DAC at each AP site, and it is also beneficial to reduce power consumption and implementation scale of each site. Then, it can relax the installation requirements at an antenna site. As one type of ARoF, we have focused on intermediate frequency over fiber (IFoF) [3]. The RF waveform is converted to the IF and then converted to optical signals, and the optical signal is converted to IF and then converted to RF signal at AP site. Applying different IF to convert each signal stream for a MIMO layer, it can be multiplexed by FDM in a single optical fiber, which drastically improve efficiency. In case of cell-free massive MIMO, the multiplexing streams, that are

generated at the central site, are hauled to the vicinity of the AP sites with a single fiber, and then they are split to each site. That reduces the number and total length of optical fibers required to be installed. In addition, cost of the E/O and O/E converter is high for mmWave frequency band, and it can save the device cost by the conversion of the IF. This IFoF based mobile fronthaul concept has been demonstrated in [4]. In the demonstration experiment, a millimeter-wave (28 GHz) wireless communication environment was established by the 5G signaling tester, assumed as central site, multiple antennas at different position, regarded as distributed APs and commercial smartphone, with the IFoF based mobile fronthaul. In the communication tests, the link among central site and the smartphone through the fronthaul and wireless propagation channel is established successfully. Then, it is confirmed that the stable throughput can be obtained even under the tree blockage by the macro diversity effect with the distributed APs.

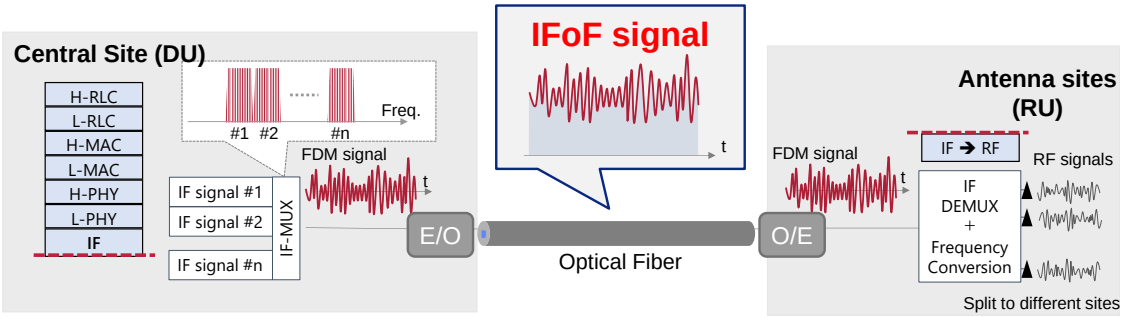

Fig.1-2 Concept of IFoF based mobile fronthaul

1.4 Pilot decontamination for capacity enhancement of cell-free massive MIMO

In the large-scale cell-free massive MIMO, it is required to accommodate a large number of UEs and capability to higher order spatial multiplexing is desired. Due to the degrees of freedom of the large number of distributed antennas, it has a potential to multiplex a large number of UEs. However, the overhead of the reference signals could be a bottleneck to increase the number of spatial multiplexing. For example, current 3GPP standard utilizes orthogonal demodulation reference signal (DMRS), and its number of ports is limited to 24 in 3GPP at the end of rel.18. Therefore, reuse of the reference signal is inevitable for that purpose, which eventually induces pilot contamination, and the total capacity cannot be increased due to the severe channel estimation error. In addition, cell-free massive MIMO has no clear boundaries in an area, it is hard to apply a cell-based pilot reuse restriction.

To resolve the pilot contamination issue, we have investigated a digital signal processing-based pilot decontamination scheme, which accepts reuse of the identical pilot between UEs. Fig. 1-3 shows a concept of the proposed pilot decontamination method and its simulation results. The proposed method exploits difference of antenna

correlation between same-pilot UEs due to the received angle difference. In the receiver, the contaminated pilot is transformed into angle domain, then a target pilot and interference pilot are separated in the angle domain. The proposed decontamination requires estimation of antenna correlation information as angle domain information in advance. The simulation was conducted with parameters that area size is 2×2 km^2, the number of APs is 25, the number of antennas at each AP is 16, and the carrier frequency is 3.5 GHz, respectively. We adopted two types of pilot assignment method, one is random assignment, and the other is the assignment minimizing contamination under the decontamination method [5]. In the case of random assignment without our decontamination method, the sum SE decreases as the number of UEs increases, due to the channel estimation error caused by the contamination. On the other hand, the case of random assignment with decontamination improves the sum SE compared with conventional case. Furthermore, the sum SE of decontamination with ingenious assignment approaches to that of ideal estimation.

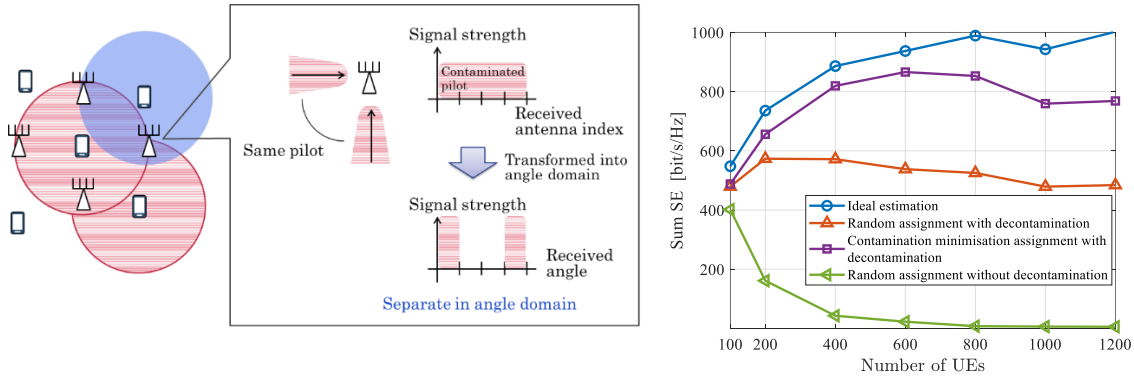

(a) Concept of pilot decontamination (b) Simulation results

Fig. 1-3 Pilot decontamination for increasing capacity in cell-free massive MIMO

1.5 Energy efficiency improvement for AP on/off switching

For many years, spectral efficiency (SE) has been the primary performance indicator in mobile communication systems. Recently, however, energy efficiency (EE) is also paid attention to by both academia and industry as a key performance indicator of 6G. In large-scale cell-free massive MIMO, since the huge amount of energy would be consumed in the whole network, the EE improvement is requisite. Most general way to improve EE is reduction of power consumption because EE is given as data rate (multiplication of bandwidth and SE) divided by power. Note that, when we maximize EE, a constraint of minimum SE is needed to guarantee a certain level of SE since there is a trade-off between improving SE and reducing power.

One promising technique to improve EE of cell-free massive MIMO is AP on/off switching. This adaptively puts the APs into sleep mode, which have little contributions

to the performance of UEs according to the multiplexed UEs at each moment as shown in Fig. 1-4(a). Color lines denote the user centric cluster for each UE, and the gray AP is in sleep mode. To establish an efficient scheme, we have investigated efficient algorithms for joint processing with the AP on/off switching and UCC to improve EE under the constraint about required data rate of UEs [6]. A performance of total EE is shown in Fig. 1-4(b). Red solid line shows the performance with the proposed greedy ASO algorithm. The proposed algorithm executes ASO and UCC alternately to obtain better EE performance with realistic computational complexity. On the other hand, blue line shows the performance with conventional ASO algorithm, where fixed number of APs are put into sleep mode in advance of UCC. As can be seen from Fig. X-4(b), 50-percentile of the performance is improved by 92%.

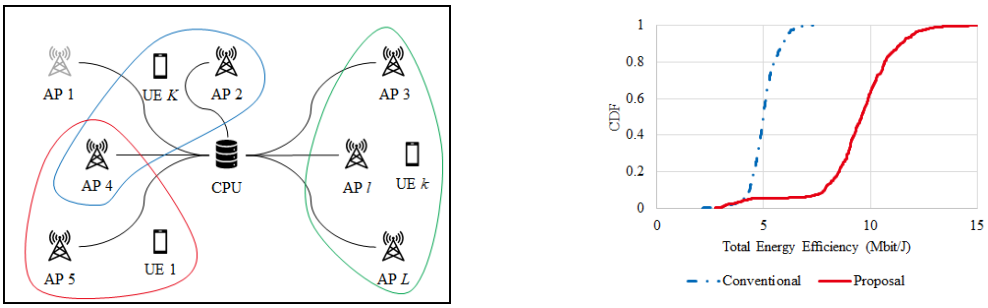

(a) Concept (b) Simulation results

Fig. 1-4 AP on/off switching for Cell-Free massive MIMO

1.6 Conclusion

In this article, research activities for deploying large-scale cell-free massive MIMO are introduced. Concretely, the following topics are introduced: (1) user centric clustering to have scalability and its demonstration trial, (2) IFoF based mobile fronthaul technology to reduce deployment cost, (3) pilot decontamination scheme to increase the capacity for increasing the number of spatial multiplexing, (4) AP on/off switching control for energy efficient operation. Including these technologies, it is expected to evolve standard to operate cell-free, or distributed MIMO, more effectively in 3GPP, O-RAN, etc.

Acknowledgements

The part of the contents are obtained from the commissioned research (JPJ012368C00401) by National Institute of Information and Communications Technology (NICT), Japan.

REFERENCE

[1] ITU-R, M2516-0, “Future technology trends of terrestrial international mobile telecommunications system towards 2030 and beyond,” Nov. 2022.

[2] KDDI Research Inc., “Successful outdoor experiment employing User-centric RAN that can provide stable communication to each customer in the area,” https://www.kddi-research.jp/english/newsrelease/2023/052302.html
[3] S. Ishimura, B. G. Kim, K. Tanaka, K. Nishimura, H. Kim, Y. C. Chung, et al., "Broadband IF-over-fiber transmission with parallel IM/PM transmitter overcoming dispersion-induced RF power fading for high-capacity mobile fronthaul links", IEEE Photonics J., vol. 10, no. 1, Feb. 2018.
[4] KDDI Research Inc., "World first successful demonstration of wireless network deployment methodology for Beyond 5G," Oct. 2021. (Press Release) https://www.kddi-research.jp/english/newsrelease/2021/100701.html
[5] N. Osawa, F. Göttsch, I. Kanno, T. Ohseki, Y. Amano, K. Yamazki, and G. Caire, “Overloaded Pilot Assignment with Pilot Decontamination for Cell-Free Systems,” in Proc. IEEE WCNC 2023, April 2023.
[6] M. Ito, I. Kanno, Y. Amano, W. Y. Chen, T. Choi, and A. F. Molisch, “Joint AP On/Off and User-Centric Clustering for Energy-Efficient Cell-Free Massive MIMO Systems,” in Proc. IEEE VTC 2022 fall, Sep. 2022.

2 High-frequency Band Distributed Antenna System

NTT Access Network Service Systems Laboratories, Daisei Uchida
NTT Access Network Service Systems Laboratories, Takuto Arai
NTT Access Network Service Systems Laboratories, Shuki Wai
NTT Access Network Service Systems Laboratories, Mizuki Suga
NTT Access Network Service Systems Laboratories, Hideki Toshinaga
NTT DOCOMO 6G Network Innovation Department, Satoshi Suyama
NTT DOCOMO 6G Network Innovation Department, Juling Huiling
NTT DOCOMO 6G Network Innovation Department, Kiichi Tateishi

Abstract— **This article introduces a high-frequency band distributed antenna system that achieves 100 Gbps or more, which is the target of extreme-high-speed and extreme communication capacity wireless transmission for 6G. Specifically, we describe the system concept and required technologies. Moreover, we introduce the demonstration experiment results of A-RoF technology, beam selection technology for ultra-narrow beams, and distributed cooperative MU-MIMO technology using analog beams as a study of the required technologies.**

2.1 Introduction

100Gbps or more is currently the 6G target for extreme high speed and high communication capacity [1]. To stably achieve wireless transmission speeds of 100 Gbps or more, a signal bandwidth of 1 to 10 GHz is required, making it necessary to utilize the millimeter wave (mmWave) to sub-terahertz (Sub-THz) bands [1].

This article introduces a high-frequency band distributed antenna system as a promising means of utilizing these high frequency bands for mobile communications. We describe the system concept, the required technologies, and a study of the issues involved.

2.2 High-frequency Band Distributed Antenna System

Since the sub-terahertz band emphasizes direct links more than millimeter waves, it is necessary to arrange base stations to ensure “line of sight (LoS)” rather than “proximity”. A distributed antenna system is expected to achieve this [1-2]. Figure.2-1 shows the system concept of this system. A base station (BS) consists of one central station (CS) and multiple distributed antennas (DAs). DAs are set in a distributed manner so that radio waves can propagate in multiple directions to provide terminal coverage, and radio signals transmitted or received at any antenna can be modulated and demodulated by one CS. By switching antennas at the L1 layer, this system can achieve stable high-frequency band wireless transmission even in the fluctuating shielding environments created by human bodies and cars, etc. Furthermore, by providing site diversity from multiple directions, this system is also expected to realize

DAs placement designs that significantly reduce shielding loss margins while realizing uniform wireless transmission quality within the services area.

We believe that three technologies are required to realize this system. Figure. 2-2 shows conceptual diagrams of these technologies. The first is distributed antenna deployment to ensure LoS propagation paths, with high probability for mobile terminals. The second is distributed propagation realized by the switching of communication established on ultra-narrow beams to follow the movement of user terminals. The third is distributed cooperative MIMO, which utilizes path control technology to handle the large-capacity simultaneous transmission demanded by many user terminals [1]. In the next chapter, we describe a study on each technology.

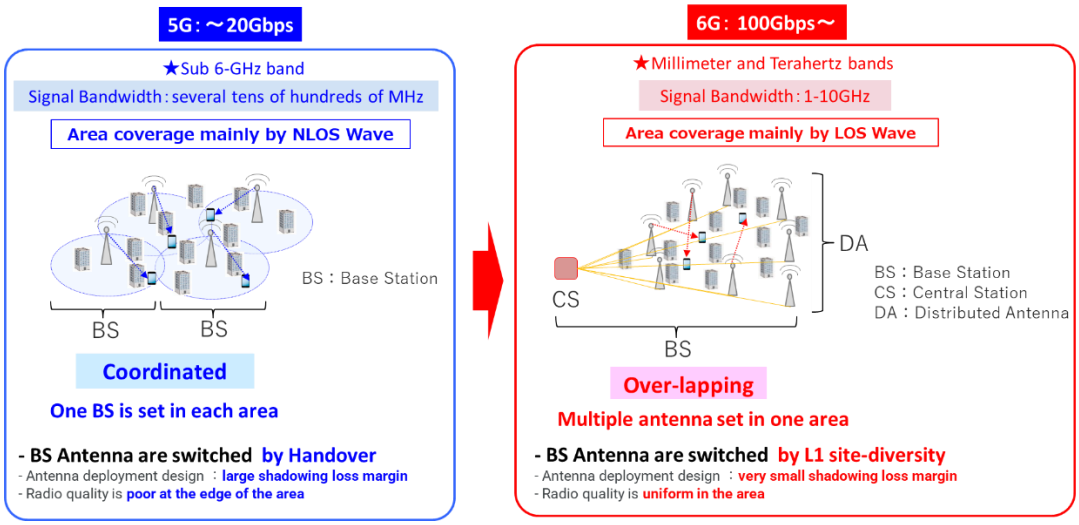

Fig. 2-1 High-Frequency Band Distributed Antenna System

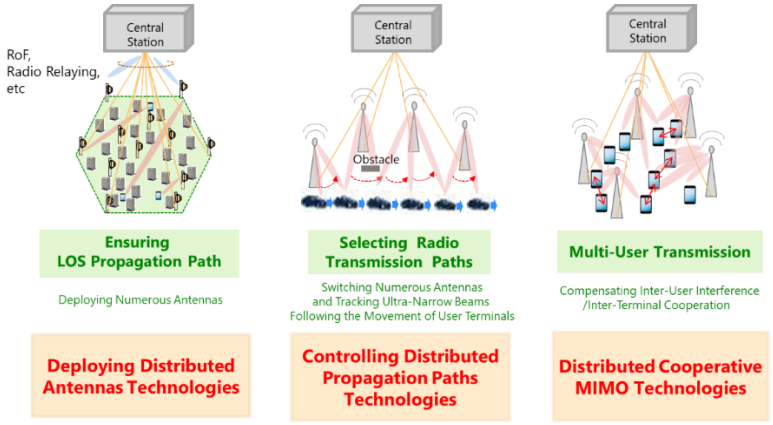

Fig. 2-2 Technologies issues for high-frequency band distributed antenna system

2.3 Deploying Distributed Antennas Technologies

We describe analog radio over fiber (A-RoF) as a means of implementing DAs technologies. A-RoF is highly effective way of connecting a large number of DAs to a CS in distributed antenna systems. Studies have been conducted to apply A-RoF to distributed antenna systems [3-4]. Compared to coaxial cables, connecting DAs and CS with optical fiber offers the significant advantages of low attenuation and long-distance transmission of wireless signals, especially in high frequency bands. Furthermore, analog-digital conversion functions can be reduced compared to conventional BS, because wireless signals are directly converted into optical signals without analog to digital conversion. This is expected to realize DAs that are smaller and have lower power consumption.

To confirm the feasibility of A-RoF for application to actual wireless systems, a 5G signal transmission experiment was conducted [5]. Experimental overview and results are shown in Figure. 2-3. Optical signals were transmitted via 20km single mode fiber (SMF) using C band. The signal was received by the receiver antenna after 6.3m air transmission. The wireless signals used the 5G FR2 signal format, and so had 28.25GHz center frequency, 100MHz bandwidth, 60kHz subcarrier spacing and 64QAM modulation format.

The measured results confirmed the impact of A-RoF transmission on signal quality. The error vector magnitude (EVM) value after 20km A-RoF transmission was 2.39% and the 5G signals finally received after 6.3m air transmission had EVM value of 2.71%. These results reveal that the measured EVM values after 20km A-RoF and 6.3m air transmission are sufficient meet 3GPP requirement of 8% or less for the 64QAM format. The experiments confirm that A-RoF has the potential to realize effective high-frequency band distributed antenna systems.

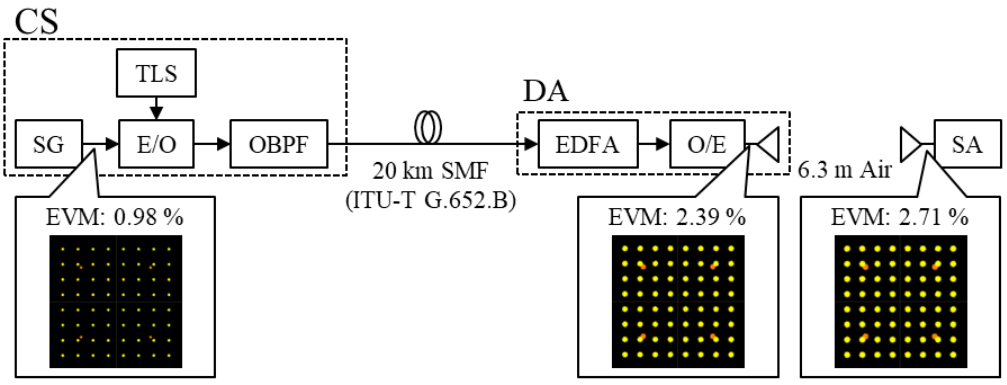

SG: signal generator, TLS: tunable laser source, E/O: electric-optic convertor, OBPF: optical band pass filter
EDFA: erbium-doped fiber amplifier, O/E: optic-electric convertor, SA: spectrum analyzer

Fig. 2-3 Experimental overview and results.

2.4 Control of Distributed Propagation Paths

We introduce two analog beam controlling technologies to permit the manipulation of the distributed propagation paths.

2.4.1 Fast Beam Search Based on Recorded Beam Combinations [6]

When conducting beam search in a high-frequency band distributed antenna system, radio resources used the beam search are consumed in proportion to the number of DAs. In order to solve this problem, we are considering a method that does not search all beams for all DAs except one DA. Figure. 2-4 shows the concept of this method. Owing to the dominance of LoS paths in this system, optimal beam combinations of each DA for a user equipment (UE) depend on the UE position, and so the combination is expected be limited in entire area. Based on this consideration, we have assessed a beam search method that considers only those beam combinations selected at each DA in the past. After detecting the optimal beam for the first DA, the other DA searches consider only those beam that were selected in the past when the first antenna's beam was selected as the optimal beam.

We evaluated the number of beam searches and the downlink transmission capacity of the selected beams using this method. Figure 2-5 shows the simulation results. The simulation model is as follows. In a 100m×100m×15m area, DAs are set on the ceiling at equal intervals and a UE is randomly set across the area. The carrier frequency band is the 100-GHz band and the signal bandwidth is 8GHz. The DA has 2-dimensional array antenna with 16×16 elements while the UE is equipped with 2 antennas. The channel model is free space propagation. It was assumed that beam combinations would be sufficiently recorded for the entire area. Fig.2-5 shows that this method can reduce the number of beam searches by more than half while maintaining the downlink transmission capacity compared to the method of hierarchical searching beams for all DAs.

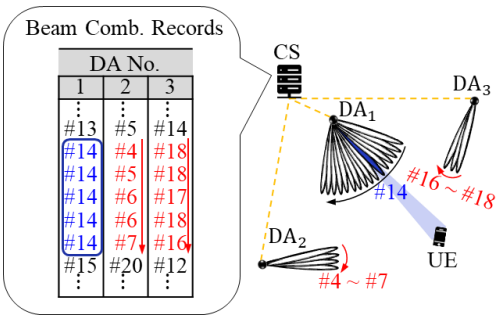

Fig. 2-4 Proposed partial beam search based on recorded beam combinations.

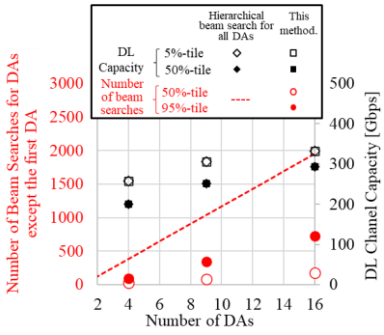

Fig. 2-5 The number of search beams versus the number of DAs

2.4.2 Beam Search Method with Adaptive Beam Width Control Based [7]

We are considering a beam search method that adaptively changes the beam width according to distance from the DA to the obstacle blocking high-frequncy band transmission , such as a building. The concept of this method is shown in Fig. 2-6. This method realizes fast initial access by reducing the number of candidate beams used in beam search by widening the beam width according to the distance to each obstacle.

We have conducted an experiment on this method by using a 60-GHz band radio device compliant with IEEE 802.11ad. Figure 2-7 shows the Received Signal Strength Indication (RSSI) at each measurement point when using this method. In this method, the beam width was changed to 16 degrees, 26 degrees, and 42 degrees depending on the distance of the obstacle. For comparison, RSSI were also measured with the beamwidth fixed in all directions. In the method shown in Fig.2-7, the arrow directions and colors represent the beam direction and beam width. The red, green, and blue lines represent beam width of 16deg., 26deg., and 42deg., respectively. As shown in Fig. 2-7, this method can reduce the number of beam searches from 25 to 12 while maintaining almost the same RSSI value compared to when the beam width is fixed at 16 degrees. Therefore, this method can maintain the size of the coverage area while reducing the overhead incurred by beam search.

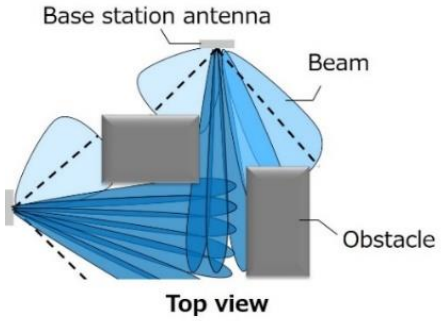

Fig. 2-6 Concept of this method.

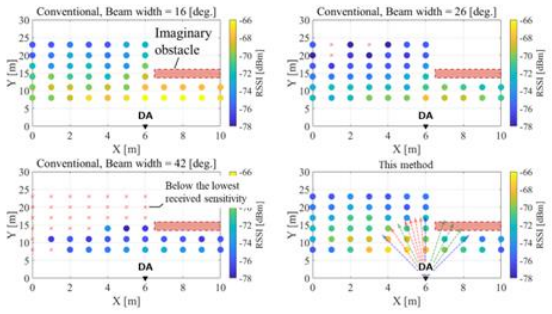

Fig. 2-7 RSSI measurement result when using this method and when beamwidth is fixed.

2.5 Multi-user Transmission by analog beamforming formed DAs as Distributed Cooperative MIMO [8]

We describe multi-user transmission demonstration experiment that used a 40-GHz band distributed antenna prototype to study distributed cooperative MIMO technologies.

If interference between UEs can be suppressed by DAs, this system can provide multi-user transmission to UEs by connecting them to as many DAs as possible. Pre-coding is a conventional technique for suppressing the interference between UEs. However, when multiple DAs are used for pre-coding, the positions at which the interference can be canceled are constricted, making it difficult to suppress the interference experienced by UEs.

Against this background, we conducted a demonstration experiment of multi-user transmission by the analog beamforming functionality of DAs to achieve wide directional interference suppression. This experiment was conducted in a laboratory with 4 pillars in an area of 29m ×15m. The frequency band used in this experiment was 40-GHz band, which is higher than the 28 GHz band of 5G mmWave service in Japan. Fig. 2-8 shows the experimental parameters and results. When pre-coding was applied with wide beams at both DAs and the UE antennas, the downlink channel capacity decreased by 90% when the UEs moved. On the other hand, when narrow analog beams were implemented at both the DAs and UEs antennas without using pre-coding, there was basically no drop in channel capacity from the stationary UE case.

The experimental parameters

Experiment Area	29m x 15m (Indoor)
Frequency band	40-GHz
Signal Band	100MHz
Wireless transmission scheme	5G NR OFDM (SCS:60KHz)
The number of distributed antennas	14
The number of UEs	4
The number of data streams per UE	2
Pre-coding updated cycle	40ms
Narrow Analog beam (Narrow beam)	Beamwidth : 16 degree Beam Sweep: -67 to 67 degrees Beam Gain : equal to Wide beam
Wide Analog beam (Wide beam)	Beamwidth : 60 degree Fixed beam Beam Gain : equal to narrow beam
Pre-coding	block diagonalization
Post-coding	MMSE

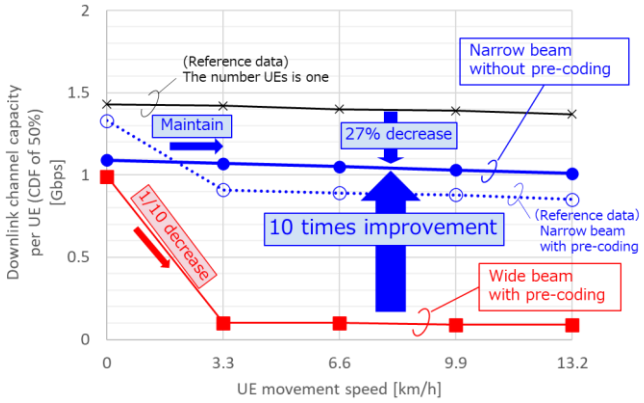

Fig. 2-8 The experimental results of multi-user transmission using 40-GHz Distributed Antenna system prototype

2.6 Conclusion

We described a high-frequency band distributed antenna system as a means of realizing extreme high speed and large communication capacity wireless transmission that achieves 100 Gbps or more for 6G. We introduced and described its required technologies and studied their issues.

Acknowledgements

We are grateful to NEC Corporation for their collaboration in the early stages of this work.

REFERENCE

[1] NTT DOCOMO, INC, "White Paper 5G Evolution and 6G", January 2023 https://www.docomo.ne.jp/english/binary/pdf/corporate/technology/whitepaper_6g/DOCOMO_6G_White_PaperEN_v5.0.pdf

[2] H. Q. Ngo, et al., “Cell-free massive MIMO versus small cells,” IEEE Trans. Wireless Commun., vol. 16, no. 3, pp. 1834-1850, Mar. 2017.
[3] K. Ito, et al, “Remote beamforming scheme with fixed wavelength allocation for radio-over-fiber systems employing single-mode fiber,” IEEE JLT, vol. 40, no. 4, Feb. 2022.
[4] M. Suga, et al. ”Beam control method for analog RoF systems based on pre-beamforming with a few antenna elements,” IEICE ComEX, vol.12, no. 12, Dec. 2023.
[5] Kota Ito, et.al, “Passive beamformer based remote beamforming scheme for radio-over-fiber systems: Experimental demonstration using 28-GHz band reflectarray,” Optics Communications, vol. 513, June 2022.
[6] S. Wai, et.al, "Fast Beam Search Based on Recorded Combinations for Distributed Massive MIMO Systems Using Sub-THz Wave Bands," in IEEE Trans. Veh. Technol., vol. 72, no. 8, pp. 10263-10272, Aug. 2023.
[7] T. Arai, et.al, “A beam search method with adaptive beam width control based on area size for initial access,” in IEICE Trans. Communications, vol.E106-B, no.4, pp.359-366, April 2023.
[8] NTT, “Successful 40 GHz band distributed MIMO demonstration of maintaining radio communication quality even when interference occurs due to movement of multiple users ~ Progress in realizing high-capacity communications at event venues and factories where many radio terminals are active ~”
https://group.ntt/en/newsrelease/2023/10/31/pdf/231031aa.pdf

3 Real-Time Simulator for 6th Generation Mobile Communication System Using Distributed MIMO

Kiichi Tateishi, NTT DOCOMO, INC.
Satoshi Suyama, NTT DOCOMO, INC.
Huiling Jiang, NTT DOCOMO, INC.

Abstract— **The 6th generation mobile communication system (6G) is expected to realize extremely high-data-rate and high-capacity communications with a peak data rate of more than 100 Gbps. In order to realize 100 Gbps extremely high-data-rate communications in 6G, the utilization of so-called sub-terahertz bands such as 100~300 GHz band, which can utilize a dramatically wider signal bandwidth compared to 5G, is examined. We have developed a 6G system-level simulator (6G simulator) to clarify the feasibility of 100 Gbps extremely high-data-rate communications by utilizing the sub-terahertz band as a system. In this article, we introduce an overview of the functions of this simulator and examples of performance evaluation with distributed MIMO (Multiple Input Multiple Output) technology in outdoor city environment.**

3.1 Introduction

In 6G, one of the goals is to provide extremely high-data-rate communications exceeding 100 Gbps, and to this end, the use of the sub-terahertz band from 100 to 300 GHz is being studied.

NTT DOCOMO has been developing a 6G system-level simulator to evaluate 6G system performance when using the sub-terahertz band. New Radio Network Topology (NRNT) for constructing distributed radio network topology in the space domain is becoming an important technical area [1][2]. In NRNT, a variety of technologies are being studied including distributed MIMO, use of existing objects such as streetlamps and lighting fixtures for mounting antennas, development of advanced repeater technology, use of Reconfigurable Intelligent Surface (RIS) reflectors that can dynamically control reflection intensity and direction, the use of moving Base Stations (BSs) , and Mobile Station (MS)-to-MS linking, all of which refer to nodes configuring a network topology and the technologies adopted for them [1]. This article describes the 6G simulator that introduces distributed MIMO in an outdoor urban environment.

3.2 Overview of 6G Simulator

6G simulator was developed to quantitatively test the 6G requirements and technical concepts described in NTT DOCOMO's 6G white paper [1] and to test the possibility of applying the sub-terahertz band from a system perspective [3][4].

This simulator introduces distributed MIMO at the BS for both the Downlink (DL) and Uplink (UL). In distributed MIMO, a BS consists of multiple Transmission and

Reception Points (TRPs) corresponding to BS antennas and a central station that consolidates those TRPs. Here, throughput can be improved through cooperative transmission/reception at multiple TRPs. In the case of not applying distributed MIMO, MS performs transmission/reception with only one TRP. This simulator installs multiple TRPs fixed to positions established beforehand and evaluates DL and UL throughput characteristics of each MS during (cooperative) transmission/reception between those TRPs and the MS. In addition, this simulator provides services while a drone TRP moves along a specific path to reduce propagation loss due to blocking. Robots and self-driving vehicles are also arranged as MSs in addition to devices possessed by people.

This simulator introduces a massive MIMO antenna consisting of multiple sub-arrays at each TRP. To simplify the evaluation, it is assumed that the reflection direction by an RIS reflector can be ideally controlled. In short, the simulator uses the received power calculated in the above way to ideally switch to the TRP that can communicate with the MS without delay.

When applying distributed MIMO, transmit precoding will be executed for the sub-arrays of all TRPs under the central station, but when not applying distributed MIMO, transmit precoding will be executed only among the sub-arrays within a TRP.

In this article, the simulator uses a Singular Value Decomposition (SVD) precoder for transmit precoding. The SVD precoder performs an eigenvalue decomposition on the covariance matrix of the channel matrix and extracts eigenvalues from that matrix in descending order only for a number of rows corresponding to the number of MIMO layers of all MSs being allocated resources.

Reception processing at each TRP and MS performs signal detection by a receiver in which the Minimum Mean-Squared Error (MMSE) norm using the channel matrix is used as a basis for Interference Rejection Combining (IRC) (MMSE-IRC receiver). This simulator computes the block error rate from the received SINR of the detected signal and calculates throughput on the DL and UL.

3.3 6G Simulator Using Distributed MIMO in an Outdoor Urban Scenario

This simulator simulates an outdoor urban environment. It can execute a simulation-based evaluation at the system level in a scenario that deploys 5G and 6G in such an environment. The urban scenario is shown in Fig. 3-1. This environment includes an open public square surrounded by high-rise buildings. The square includes no reflecting objects but is lined with trees. People, robots, and self-driving vehicles are either stationary or moving. Fixed TRPs and RISs are installed on the walls of buildings or on streetlamps and a drone TRP makes a round trip in the air along a roadside to provide services to MSs situated away from buildings in the square.

Simulation assumptions are listed in Table 3-1. The center frequency of Sub6,

millimeter-wave, and sub-terahertz is 4.7 GHz, 28 GHz, and 100 GHz, respectively. The massive MIMO antenna of a TRP uses a planar array and consists of nine sub-arrays, each of which performs analog beamforming (BF) of a single beam by an analog circuit.

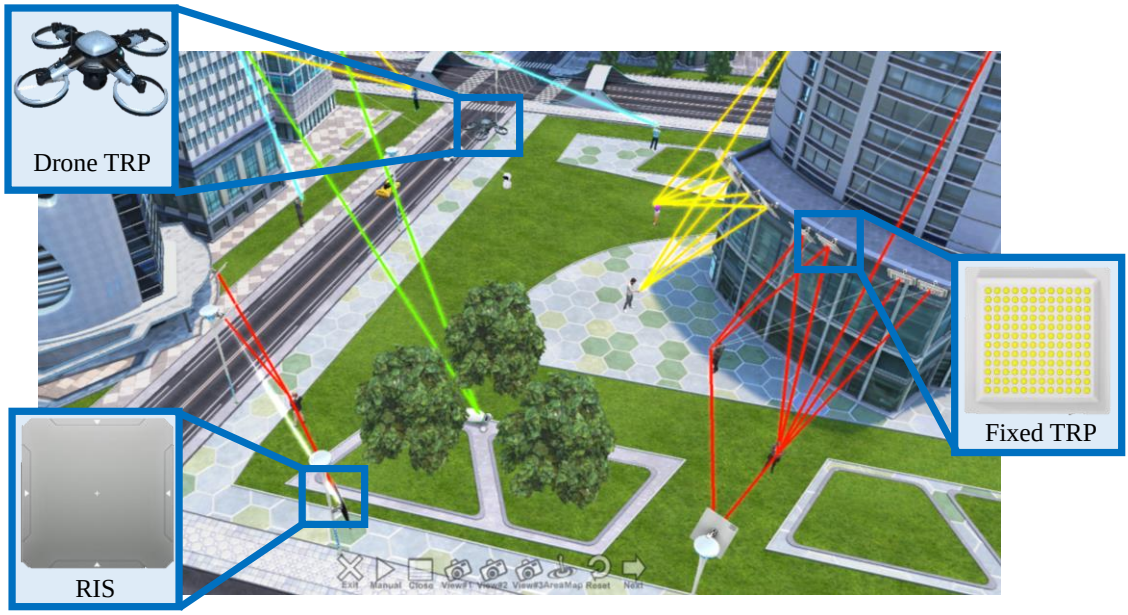

Fig. 3-1 6G simulator in an urban scenario.

The duplex mode used here is Time Division Duplex (TDD) with a DL/UL time ratio of 7:3 across all slots. This evaluation environment consists of an arrangement of 22 MSs with 18 persons possessing an MS and the remaining four MSs mounted on two robots and two self-driving vehicles. People and robots are moving at 3 km/h while self-driving vehicles are moving at 60 km/h, both without stopping. In the sub-terahertz band, it is assumed here that a throughput generally greater than 100 Gbps can be achieved with 4 or more layers. The propagation environment is a multipath rayleigh fading channel model in which spatial correlation among antenna elements is given according to TRP and MS positions and the antenna configuration.

Table. 3-1 Simulation assumptions

	Sub6	**Millimeter wave**	**Sub-terahertz**
Center frequency / Bandwidth	4.7 GHz / 100 MHz	28 GHz / 400 MHz	100 GHz / 8,000 MHz
Number of antenna elements in TRP (vertical × horizontal × sub-arrays)	144 (4×4×9)	2304 (16×16×9)	9216 (32×32×9)
Total transmission power in TRP	30 dBm		
Sub-array spacing	0.5 λ	4 λ	30 λ
TRP antenna element gain	5 dBi		
MS transmission power	23 dBm		
Number of antenna elements in MS (vertical × horizontal × sub-arrays)	144 (4×4×9)		
MS antenna spacing	0.5 λ		
Number of MIMO layers	1, 2, 3, 4, 8		

The results of the MS throughput ratio when not applying distributed MIMO are shown in Fig. 3-2. The graphs at the left of the figure show throughput ratios for the DL and UL. Here, the throughputs of 0–1 Gbps, 1–10 Gbps, 10–50 Gbps, 50–100 Gbps, and 100 Gbps or greater are expressed as five different colors with the horizontal axis and vertical axis representing time (slot number) and throughput ratio, respectively. The colors of the straight lines connecting a TRP and MS in the figure correspond to these throughput colors. The graph at the right of the figure shows the throughput for User Equipment (UE) #22 positioned in front of a high-rise building and circled in black with the horizontal axis and vertical axis representing time (slot number) and throughput, respectively.

From Fig. 3-2, the graphs at the left of the figure show that about 70% of the MSs could achieve a throughput over 1 Gbps in the DL while about 9% could achieve a throughput over 100 Gbps. The graph at the right of the figure shows that UE #22 could stably obtain a throughput over 100 Gbps in the DL. Users in good environments could enjoy throughputs exceeding 100 Gbps thanks to the effects of greater bandwidths in the sub-terahertz band.

Next, Fig. 3-3 shows evaluation results when applying distributed MIMO for the same installation positions in Fig. 3-2. The graphs at the left of the figure show that about 90% of the MSs could achieve a throughput over 1 Gbps in the DL while about 18% could achieve a throughput over 100 Gbps. The graph at the right of the figure shows that the throughput of UE #22 was greater than 100 Gbps in the DL increasing to 190 Gbps at peak time. These results demonstrate that significantly higher throughput could be achieved compared with the case of not applying distributed MIMO (Fig. 3-2).

The above simulation results clarify that throughput can be greatly improved by applying distributed MIMO even in an environment in which a spatial multiplexing

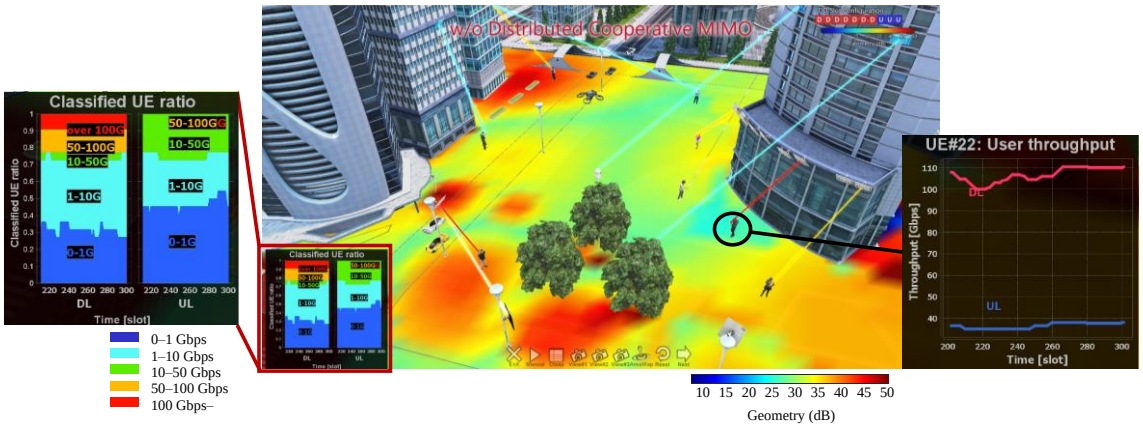

Fig. 3-2 Evaluation results without distributed MIMO.

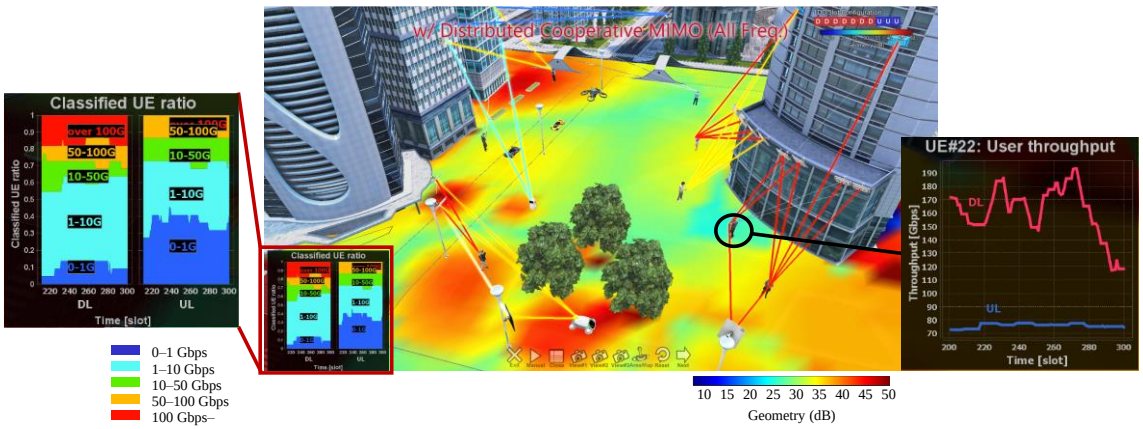

Fig. 3-3 Evaluation results with distributed MIMO.

effect by MIMO cannot be expected due to a relatively small number of reflected waves and many LOS environments as in an urban scenario.

3.4 Conclusion

In this article, we described the development of 6G simulator that introduces distributed MIMO in an outdoor urban environment. Looking to the future, we will continue to enhance our 6G simulator so that the performance of various 6G technologies can be evaluated and visualized on the system level and use cases of the 6G era can be virtually experienced based on that performance.

REFERENCE

[1] NTT DOCOMO: "5G Evolution and 6G White Paper, Version 5.0," Jan. 2023. https://www.docomo.ne.jp/english/binary/pdf/corporate/technology/whitepaper_6g/DOCOMO_6G_White_PaperEN_v5.0.pdf

[2] Y. Kishiyama et al.: "Trends and Target Implementations for 5G evolution & 6G," NTT DOCOMO Technical Journal, Vol. 23, No. 2, pp. 4–13, Oct. 2021.

[3] T. Okuyama et al.: "6G System-level Simulator—Toward 100 GHz Band, 100 Gbps Extreme-high-data-rate Communications—," NTT DOCOMO Technical Journal, Vol. 23, No. 3, pp. 13–26, Jan. 2022.

[4] K. Tateishi et al.: "Enhancement of 6G System-level Simulators," NTT DOCOMO Technical Journal, Vol. 25, No. 2, Oct. 2023.

4 Distributed MIMO Technologies for High Frequency Bands

Kazushi Muraoka, NEC Corporation
Jun Shikida, NEC Corporation
Masaaki Tanio, NEC Corporation
Toshiki Takeuchi, NEC Corporation
Yasushi Maruta, NEC Corporation

Abstract—**We present key technologies for realizing distributed MIMO in high-frequency bands. These technologies include: (1) radio over fiber transmission for cost-effective and high-quality signal transmission, (2) inter-access point coordinated transmission to reduce interference, and (3) mobility-prediction-based antenna-beam coordination for improved communication stability in the face of blocking. By integrating these technologies within distributed MIMO systems, we can facilitate stable high-capacity communication in high-frequency bands while minimizing system costs and complexities.**

4.1 Introduction

The use of high-frequency bands, such as millimeter waves, is necessary for accommodating growing mobile traffic but has a risk of communication quality degradation in the case of blockage. Distributed MIMO, which generates line-of-sight paths from access points (APs) to mobile terminals (MTs) by deploying multiple APs, is promising for overcoming this challenge. In the Beyond 5G era, it is expected that such distributed MIMO will be deployed over a wider area, with effectively coordinated multiple APs connected to a centralized baseband unit (BBU). These APs can be installed outdoors on utility poles, traffic signals, streetlights, etc., and indoors on walls and ceilings. With distributed MIMO, MTs can redundantly have line-of-sight paths from multiple APs, enhancing the communication stability of high-frequency bands. We introduce the key technologies for distributed MIMO in high-frequency bands.

4.2 Overview of Distributed MIMO System

Fig. 4-1 shows the system concept of distributed MIMO employing analog beamforming at APs. To deploy distributed MIMO over a wide area, it is necessary to install numerous APs. Securing installation sites for APs is not easy, as it can be both time-consuming and costly. Thus, it is critical to miniaturize the APs and increase the number of potential installation sites. The low-layer functional split, in which the digital signal processing functions traditionally handled by the 5G radio units (RUs) are transferred to a BBU, is suitable for AP miniaturization. In this case, communication between the fiber-optic connected APs and the BBUs requires radio over fiber (RoF) transmission, which transmits radio signal waveforms over optical fibers. If commercial-

off-the-shelf (COTS) optical transceivers can be used for RoF transmission, the installation cost can be reduced. In Section 4.3, we discuss RoF technology [1][2] that achieves high-quality transmission using COTS optical transceivers.

While installing a large number of APs over a wide area can redundantly secure the line-of-sight paths, excessive interference may occur in some locations. Therefore, distributed MIMO requires transmission technology that coordinates multiple APs to suppress interference. To coordinate transmission from the multiple APs, BBUs need to understand the received signal level of each AP and each beam at the MTs. However, in actual mobile communication systems, there is a limit to the number of reports of the received power from MTs. In Section 4.4, we will discuss inter-AP coordinated transmission [3] that is achievable even with a limited number of reports.

Furthermore, in high-frequency bands, the received power may suddenly drop, and the connection may be disrupted if an MT goes behind an obstacle. If MTs could always connect to multiple APs, received power could be maintained, but it would also result in wasting radio resources and consuming unnecessary power. Hence, we will introduce the mobility-prediction-based antenna-beam coordination [4][5], which performs selection of the combination of APs and beams based on predicting the degradation in reception quality and allows for joint transmission from multiple APs only when necessary, in Section 4.5.

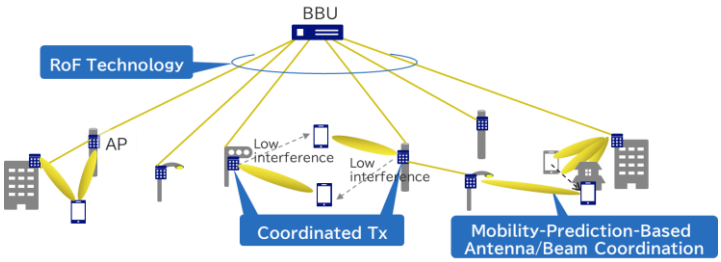

Fig. 4-1 Overview of Distributed MIMO System

4.3 RoF Transmission

Among the low-cost RoF methods using COTS optical transceivers, Delta-Sigma RoF is one of the promising approaches. To make Delta-Sigma RoF more practical, we introduce the pulse distortion model (PDM)-embedded Delta-Sigma RoF, which compensates for signal quality degradation caused by waveform distortion.

Delta-Sigma modulation is a modulation technique that outputs quantized signals, with a feedback configuration that prevents quantization errors from occurring within the desired signal bandwidth. Delta-Sigma RoF is a RoF transmission method that applies Delta-Sigma modulation. Specifically, the radio signal is converted into a 1-bit signal sequence using Delta-Sigma modulation, then transmitted to the AP through an

optical fiber as an optical signal sequence using a 1-bit COTS optical transceiver. At the AP, the original radio signal is regenerated by removing out-of-band quantization errors with a bandpass filter (BPF). While this method is effective in reducing costs owing to the use of COTS optical transceivers, there is a challenge of signal quality degradation at the BPF in the AP, caused by waveform distortion, such as asymmetric pulse distortion, during the RoF transmission process.

To address this challenge, we present the concept of PDM-embedded Delta-Sigma RoF in Fig. 4-2 (a). In the first step of this method, the radio signal passed through the BPF is sent back from the AP to the BBU, and the PDM is generated by comparing it with the original 1-bit signal sequence of the Delta-Sigma modulation. In the second step, the PDM obtained in the first step is embedded within the feedback loop of the Delta-Sigma modulation. This approach allows for compensation of not only quantization errors but also errors caused by RoF transmission distortion, enabling 1-bit modulation that prevents RoF transmission distortion from affecting the signal quality of the demodulated radio signal.

In a RoF transmission experiment using a 1 GHz bandwidth orthogonal frequency division multiplexing (OFDM) signal, we evaluated the residual spectrum obtained by extracting the errors from the original signal within the signal bandwidth. As shown in Fig. 4-2 (b), the proposed method labeled as “w/ PDM” decreased the error power by an average of 6.0 dB compared to the conventional method labeled as “w/o PDM”, resulting in the in-band Signal to Noise Ratio (SNR) of 30.7 dB. This confirmed that the proposed method can achieve an SNR of 30 dB or higher, even for a 1 GHz bandwidth signal.

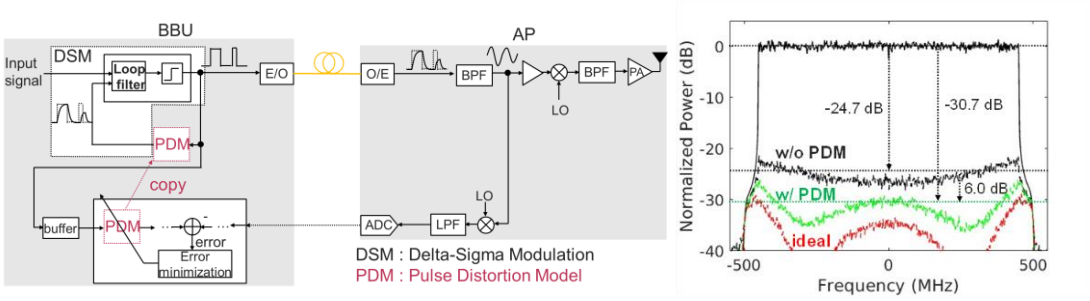

(a) Concept of PDM embedding (b) Measured 1-GHz bandwidth signal

Fig. 4-2 PDM-embedded Delta-Sigma RoF

4.4 Inter-AP Coordinated Transmission

For the inter-AP coordinated transmission method in the distributed MIMO, we adopt an approach that selects MT and beam based on the reported results of beam reception quality. Furthermore, in order to enable appropriate MT and beam selection even under conditions where the number of reports of beam reception quality is limited, we present a method utilizing a database (DB) of beam reception quality [3].

One of the inter-AP coordinated transmission methods in a distributed MIMO system adopting analog beamforming is coordinated user and beam selection. This method selects a combination of an MT and an analog beam for each AP to minimize inter-AP interference. Specifically, the selection process utilizes the beam reference signal received power (RSRP) at the MT. For each AP, the MT and beam are selected such that the difference between the beam RSRP of the serving AP and the beam RSRP of the interfering AP is greater than a threshold. This allows for reduced interference and improved user throughput performance.

However, measuring the RSRP of all beams from all APs at MTs and reporting all of them to the BBU is not feasible from an overhead perspective. Therefore, we present a method to estimate the RSRP of all beams from the reported RSRP of a limited number of beams using an RSRP DB, and use the estimated beam RSRP to select MTs and beams. Fig. 4-3 (a) shows the conceptual diagram of the RSRP DB. As shown in the figure, the average RSRP value of each beam from each AP in each area is stored in the DB. The DB is constructed by clustering the RSRP values at multiple positions based on similarity. When selecting MTs and beams for each AP, the appropriate RSRP values corresponding to the target MT are retrieved from the DB by checking the similarity between the reported RSRP of a limited number of beams and the clustered RSRP in the DB.

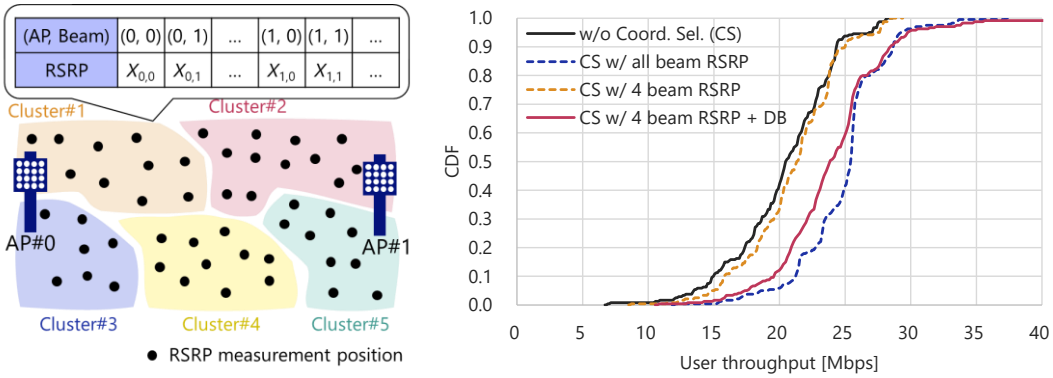

(a) Concept of RSRP DB (b) User Throughput Performance

Fig. 4-3 Coordinated MT and Beam Selection with RSRP DB

Fig. 4-3 (b) shows the user throughput performance when applying coordinated MT and beam selection using the RSRP DB. From the figure, it can be seen that when using only the RSRP of four beams without a DB, the interference reduction effect between APs is small, and the performance improvement compared to no coordinated selection is limited. However, when using the proposed RSRP DB, the performances are close to the ideal case where the RSRP of all beams from all APs are assumed to be available.

4.5 Mobility-Prediction-based Antenna-Beam Coordination

When an MT using high-frequency band moves into an environment with blockage, a sudden drop in radio communication quality or disconnection may occur as radio waves do not diffract easily. For distributed MIMO performing analog beamforming, a mobility-prediction-based antenna-beam coordination predicts the occurrence of sudden radio communication quality degradation due to blocking by predicting the subsequent position of the MT and can select the appropriate APs and beams [5].

In this method, the radio communication quality, such as RSRP, of each AP and beam at each position is measured in advance, and the combination of optimal AP and beam at each position is learned. During actual operation, the radio communication quality of each AP and beam for an MT is continuously observed, and the position of the MT is estimated using machine learning techniques. Furthermore, the subsequent position of the MT is predicted from the estimated movement track of the MT in the past, and the appropriate APs and beams before the next radio communication quality information is obtained can be predicted. As a result, even if there is a possibility that the transmission performance of the AP and beam selected based on the current radio communication quality information is drastically degraded due to the blocking triggered by the movement, this method enables stable communication by selecting the appropriate APs and beams based on the predicted subsequent position of the MT.

In an experimental environment simulating 14 APs shown in Fig. 4-4 (a), we evaluated the relative received signal strength (relative to a predetermined level in the device) of downlink transmission by using the channel estimate between each AP and terminal antenna. Fig. 4-4 (b) shows the relative received signal strength when the MT moves along the route close to the pillars shown in Fig. 4-4 (a). The received signal strength of the conventional method, which selects the AP and beam based on the current radio communication quality, decreased by about 13 dB at the position blocked by the pillar. On the other hand, in the proposed method, which selects APs and beams based on mobility prediction of an MT, the received signal strength at the same position is improved by about 9 dB compared with the conventional method.

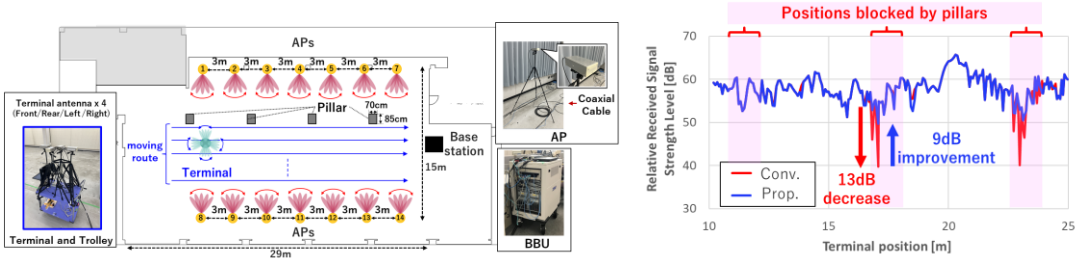

(a) Experimental environment and systems (b) Experimental results

Fig. 4-4 Experiment of mobility-prediction-based antenna-beam coordination

4.6 Conclusion

We introduced several key technologies that support distributed MIMO for the effective utilization of high-frequency bands: RoF transmission, inter-AP coordinated transmission, and mobility-prediction-based antenna-beam coordination. By combining these technologies within distributed MIMO systems, we believe it is possible to economically build systems that enable stable high-capacity communication even in high-frequency bands.

Acknowledgements

A part of this research was conducted in collaboration with NTT and NTT DOCOMO.

REFERENCE

[1] M. Tanio, N. Ishii, and K. Muraoka, "Wideband delta-sigma radio-over-fiber embedding a pulse-distortion model for beyond 5G," 2022 IEEE 96th Vehicular Technology Conference (VTC2022-Fall), 2022, pp. 1-5.

[2] Y. Kase, S. Hori, N. Oshima, and K. Kunihiro, "Radio-over-fiber system with 1-bit outphasing modulation for 5G/6G in-door wireless communication," IEICE Trans. Electron., vol.E106-C, no.7, pp.405-416, 2023.

[3] J. Shikida, K. Muraoka, T. Takeuchi, and N. Ishii, "Inter-access point coordinated user and beam selection for mmWave distributed MIMO systems," 2022 IEEE 96th Vehicular Technology Conference (VTC2022-Fall), 2022, pp. 1-5.

[4] NEC, "World's first successful demonstration of distributed MIMO that continues wireless connections in the 28 GHz band by eliminating shielding issues," https://www.nec.com/en/press/202210/global_20221031_04.html

[5] NEC, "Successful 40 GHz band distributed MIMO demonstration of maintaining radio communication quality even when interference occurs due to movement of multiple users," https://www.nec.com/en/press/202310/global_20231031_01.html

5 Distributed Antenna Technology (High-density Distributed Antenna System, and Transmission Point Sharing Control)

Takashi Dateki, Fujitsu Limited

Abstract— **This article introduces ultra-high-density distributed antenna technology for higher capacity and technology for sharing radio resources among distributed antennas deployed at multiple locations and among operators for efficient area deployment.**

5.1 Introduction

One important aspect of cell-free communication technology is to be able to flexibly provide the high communication performance of 6G when and where it is needed, depending on the user's activity and their environment. It is necessary to provide high-performance communications on demand in each local area. However, in terms of cost and power consumption, the overall processing and power consumption must be reduced to cover the entire area efficiently. This article introduces ultra-high-density distributed antenna technology for higher capacity and technology for sharing radio resources among distributed antennas deployed at multiple locations and among MNO for efficient area deployment.

5.2 Ultra-High Density Distributed Antenna

From FY2015 to FY2018, we have been engaged in research and development of ultra-high-density distributed antenna systems as a technology to realize high capacity and have performed various simulations and field experiments under the research project of the Ministry of Internal Affairs and Communications [1].

Fig. 5-1 shows an example of a computer simulation of the ultra-high-density distributed antenna system with 16 antennas in an area using the real map and building information for a part of the central Tokyo. The centralized baseband unit provides cooperative control for a large number of distributed antenna units densely located in the area. Significant system throughput improvements can be seen compared to the case where each transmission point is operated as a different cell (conventional uncoordinated system). It can also be confirmed that a good communication area is formed where the user is present without degradation at fixed cell boundaries. In general, a dense cell arrangement is expected to increase capacity, but in practice, inter-cell interference prevents a sufficient capacity increase. Therefore, we have developed a cooperative radio resource control technique that improves signal quality by reducing interference among distributed antennas. The technique is basically distributed multi-user MIMO, in which the entire signal from many distributed antennas is orthogonalized using algorithms such as ZF and MMSE, and each user receives only the signal component addressed to

each user [2]. This algorithm is called "dynamic virtual cell control technology" because of its image of forming individual cells for each user in order to improve communication quality by reducing interference for all users communicating simultaneously. Unlike conventional cell configurations that operate with fixed cell boundaries, this technology can be seen one of cell-free technologies that automatically forms virtual cells based on propagation path estimates between distributed antennas and users.

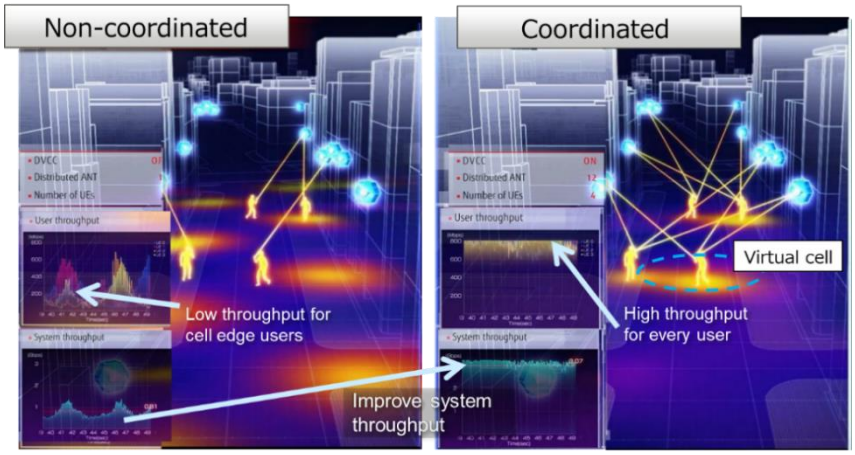

Fig. 5-1 The example simulation results of High density distribute antenna system with and without coordination control (dynamic virtual cell control)

To verify the advantage of the ultra-dense distributed antenna system, we developed the experimental device shown in Fig. 5-2(a). The base station equipment consists of a central baseband unit and up to 16 RF devices (up to 32 antennas) connected by optical fibers. The central baseband unit uses an over-the-air (OTA) calibration function to perform high accuracy channel estimation using the reciprocity between Uplink and Downlink channel, and performs spatial multiplexing transmission of up to 32 streams. A distributed antenna system using these equipment was constructed in Fujitsu Shin-Kawasaki Technology Square, Kanagawa, Japan, and indoor field experiments were performed [1]. To confirm the effect of capacity increase by coordination control of the radio resource, the system throughput was compared when the number of TPs was varied from 4, 8, to 16 under the condition that the number of TPs and the number of UEs were the same. The results are shown in Fig. 5-2(b). When cooperative radio resource control is applied, the capacity increase is almost proportional to the increase in the number of TPs, and it can be confirmed that the system capacity at 16 TPs is about 4 times larger than that of a simple small cell system (i.e. without coordination control).

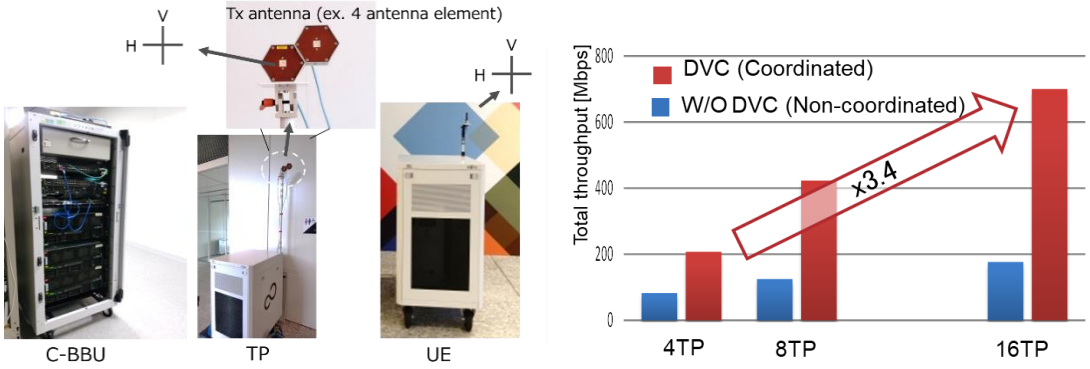

(a) (b)

Fig. 5-2 (a)The developed experimental equipment, (b) The capacity evaluation result for the increasing number of TP

The evaluation result for the case when TPs and UEs were located at one of the candidate locations is shown in Fig. 5-3(a). Fig. 5-3(b) shows the CDF of user throughput measured multiple times. The results show that distributed placement can improve the areal system capacity and that the improvement can be enhanced by appropriately designing the location of the transmission points.

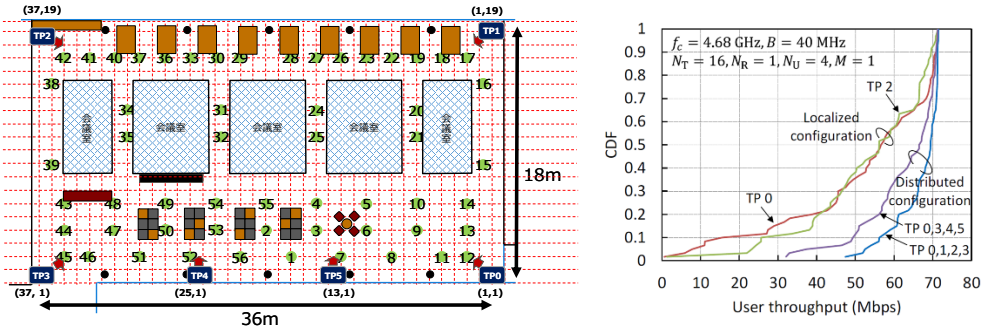

(a) (b)

Fig. 5-3 (a)Area map and the TP location, (b) CDF of the user throughput in the experimental area

5.3 Transmission point Sharing technology

In the R&D project "Research and Development of 5G Base Station Sharing Technology" by the Ministry of Internal Affairs and Communications (MIC), a technology to efficiently achieve high density in urban areas was studied by multiple Mobile Network Operators (MNO) using shared base stations located at many points in the area. In this project, the shared radio units (RUs) for multiple MNO frequencies and the radio resource control techniques that efficiently utilize fronthaul within a limited bandwidth were developed. This radio resource control is an algorithm that optimally allocates a

large number of RUs located at multiple points in multiple MNOs in an area so that high capacity can be achieved in the area while limiting the total fronthaul and radio resources below a certain value. This reduces the maximum capacity required for central baseband unit and fronthaul to process multiple cells to cover the entire area, while focusing resources on the required areas to achieve efficient communication according to data traffic demands [3],[4].

Fig. 5-4 shows an image of the operation of radio resource control in a base station sharing system. if MNO #A and #B have their own base stations in independent locations, UEs that are far from the cell center will have lower field strength. Or, in an interference-limited environment, UEs will have a lower SINR due to interference from other cells communicating in the same band. On the other hand, in a base station sharing system, each MNO allocates and uses a portion of the system bandwidth from its own location, allowing all UEs to communicate with nearby base stations without increasing the total amount of radio resources used by the entire system. This improves system performance without increasing the total amount of overall radio resources and radio transmission energy.

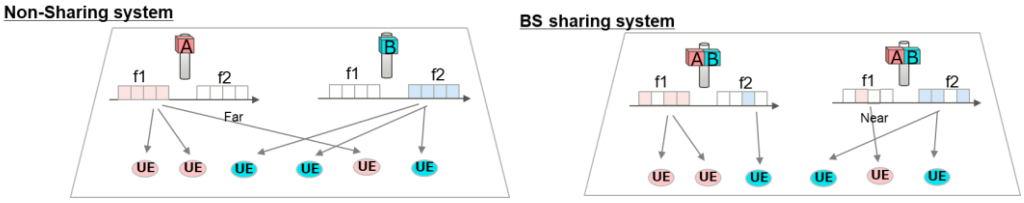

Fig. 5-4. An image of the radio resource control in a base station sharing system

Fig. 5-5 shows the simulation results of system throughput using the simulation model correspond to urban areas in 3GPP. It can be seen that the average throughput is significantly improved by base station sharing.

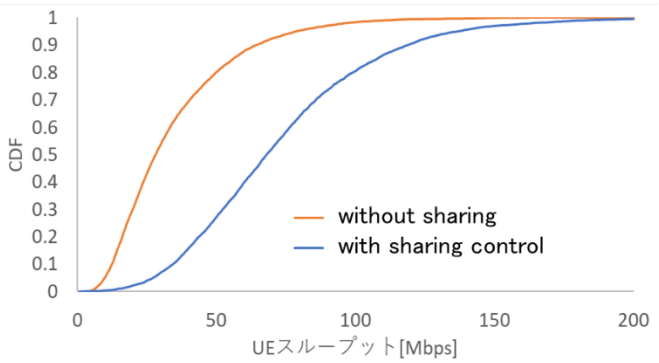

Fig. 5-5 Throughput improvement of radio resource sharing

5.4 Conclusion

In this paper, we have introduced ultra-dense distributed antenna technology for high capacity and base station sharing technology for efficient area deployment. In addition, cell free NW is also related to other technologies introduced in this white paper, such as the intelligent reflectors and relay technologies, etc. These technological elements should not only be considered separately to be introduced in different use-cases, but the integrated system including various technologies should adapt to the dynamically changing requirements of the area. The overall picture of such a 6G system has still unclear. Therefor active research and development is expected to continue in the future.

Acknowledgements

This paper includes a part of results of “The research and development project for realization of the fifth-generation mobile communications system” and “The research and development project for 5G Shared Radio Unit (JPJ000254)” commissioned by The Ministry of Internal Affairs and Communications, Japan.

REFERENCE

[1] M. Minowa et al., "5G R&D Activities for High Capacity Technologies with Ultra High-Density Multi-Band and Multi-Access Layered Cells," 2019 IEEE 89th Vehicular Technology Conference (VTC2019-Spring), Kuala Lumpur, Malaysia, 2019, pp. 1-5

[2] Takashi Seyama, Masafumi Tsutsui, Teppei Oyama, Takaharu Kobayashi, Takashi Dateki, Hiroyuki Seki, Morihiko Minowa, Tatsuki Okuyama, Satoshi Suyama and Yukihiko Okumura, “Study of Coordinated Radio Resource Scheduling Algorithm for 5G Ultra High-Density Distributed Antenna Systems,” IEEE Asia Pacific Wireless Communication Symposium (APWCS) 2016, pp.306-310, Aug. 2016.

[3] T. Kobayashi, et.al. “Function Division Type Resource Control Method for 5G Shared Radio Unit,” Proceeding of 2022 IEICE General Conference, B-5-12, Mar. 2022 , and B-5-13, B-17-5, B-5-58.

[4] T. Kobayashi, et.al., “Radio Resource Management Algorithms for Implementation in Radio Unit Sharing Systems,” IEICE Transactions on Communications J106-B (5), 327-337, 2023-05-01

6 User Cluster-centric Approach for Cell-free Massive MIMO Systems

Fumiyuki Adachi, Tohoku University
Ryo Takahashi, Tohoku University and Panasonic System Networks R&D Lab. Co., Ltd.

***Abstract*— The user cluster-centric (UCC) approach effectively improves the capacity of cell-free massive MIMO systems. This approach introduces the spatial multiplexing technique, which involves forming user clusters of neighboring users. A certain number of distributed antennas are associated with each user cluster to enable cluster-wise spatial multiplexing. Additionally, a partial interference suppression multiuser minimum mean square error (MU-MMSE) multiplexing is designed to suppress only the dominant interference from the neighboring user clusters.**

6.1 Introduction

Cell-free massive MIMO (CF-mMIMO), also known as distributed mMIMO, has recently attracted great attention as a key technology for 6G systems [1]. In CF-mMIMO systems, a central processing unit (CPU) provides communication services to users through the cooperative use of a fairly large number of distributed antennas deployed over the communication service area. To ensure system scalability and address the issue of inter-user interference, the user-centric (UC) approach is considered in [2]. In the UC approach, antenna clusters each consisting of a certain number of distributed antennas near each user are formed, and minimum mean square error (MMSE) interference suppression is applied. However, as the ratio of users to antennas increases, more users cause strong interference, thereby reducing the achievable user capacity. To address this issue, the user cluster-centric (UCC) approach is considered in [3]. This approach utilizes spatial multiplexing by associating a certain number of distributed antennas with each user cluster, consisting of neighboring users, for performing cluster-wise spatial multiplexing. Inspired by the idea of MMSE interference rejection combining (MMSE-IRC) [4], partial interference suppression multiuser MMSE multiplexing (hereafter, called partial MU-MMSE) is designed to suppress only the dominant interference from the neighboring user clusters.

6.2 UCC-based CF-mMIMO

A CF-mMIMO system model is illustrated in Fig. 6-1. A (>>1) distributed antennas are connected with the CPU via an optical mobile fronthaul to provide communication services to $U(\leq A)$ single-antenna users. The UCC and UC approaches are compared in Fig. 6-2. In the UCC approach, a user cluster consists of 3 users, and the minimum required 3 antennas are associated with this user cluster as shown in Fig. 6-2 (a). Any users outside this user cluster are interfering users for this cluster. On the other hand,

in the UC approach, each user is an interfering user to other users. An antenna cluster is formed by 2 antennas, located close to each user. This is shown in Fig. 6-2 (b).

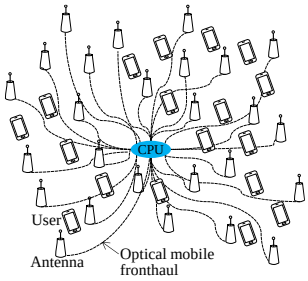

Fig. 6-1 CF-mMIMO system model.

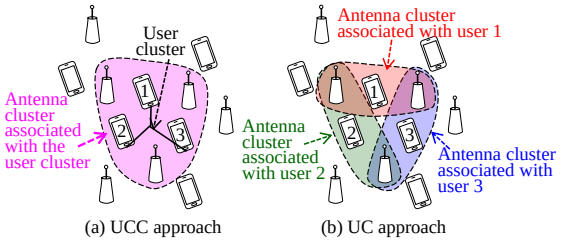

Fig. 6-2 Comparison of UCC and UC approaches.

The UCC approach takes two steps: user clustering and antenna association [3]. User clustering is done by using a constrained K-means algorithm [5],[6]. U users in the area are grouped into $K(=U/U')$ user clusters, each consisting of neighboring users, where U' denotes the number of users in each user cluster and is determined based on the computing power of the CPU. Here, for simplicity, U is assumed to be an integer multiple of U'. In antenna association, a limited number $A'(\leq A)$ of distributed antennas are associated with each user cluster to perform cluster-wise spatial multiplexing. Antenna association is based on the maximum pathloss criterion, and the same antenna is allowed to be shared by different user clusters. Let $\mathrm{M}_k \subset \{1,\ldots,a,\ldots,A\}$ with $|\mathrm{M}_k| = A'$ represents the subset of distributed antennas belonging to user cluster k. For detailed user clustering and antenna association procedures, refer to [3].

The uplink transmission model for UCC-based CF-mMIMO is illustrated in Fig. 6-3. The baseband equivalent received signal y_u of user $u(=1,\ldots,U)$ belonging to user cluster $k(=1,\ldots,K)$ is represented as

$$y_u = \mathbf{w}_u^{\mathrm{H}} \mathbf{D}_k \mathbf{h}_u s_u + \sum_{v=1, v\neq u}^{U} \mathbf{w}_u^{\mathrm{H}} \mathbf{D}_k \mathbf{h}_v s_v + \mathbf{w}_u^{\mathrm{H}} \mathbf{D}_k \mathbf{n}, \qquad (1)$$

where $\mathbf{w}_u$ is the partial MU-MMSE multiplexing weight vector of size $A\times 1$, $(.)^{\mathrm{H}}$ denotes the conjugate transpose operation, $\mathbf{D}_k = \mathrm{diag}(d_1,\ldots,d_a,\ldots,d_A)$ with $d_a = 1(0)$ if $a \in \mathrm{M}_k$ (otherwise) is the antenna association matrix for user cluster k, and $\mathbf{h}_{u(\mathrm{or}\,v)} = \left[h_{u(\mathrm{or}\,v)1} \ldots h_{u(\mathrm{or}\,v)a} \ldots h_{u(\mathrm{or}\,v)A}\right]^{\mathrm{T}}$ is the channel vector. $(.)^{\mathrm{T}}$ is the transpose operation and $h_{u(\mathrm{or}\,v)a}$ is the propagation channel gain between user u (or v) and antenna a. s_u is the baseband equivalent transmit signal with the transmit power p_u. $\mathbf{n}$ is the additive noise vector of size $A\times 1$ with each element being an independent zero-mean complex Gaussian variable having variance $2\sigma^2$.

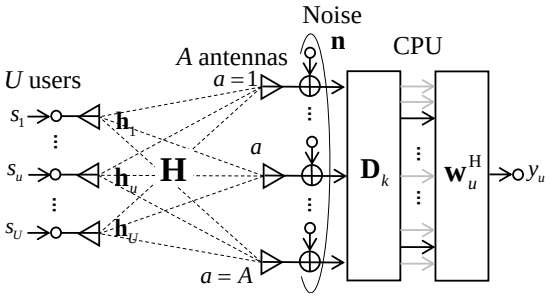

Fig. 6-3 Uplink transmission model for user u belonging to user cluster k.

The partial MU-MMSE weight vector $\mathbf{w}_u$ for uplink transmission is expressed as

$$\mathbf{w}_u = p_u \left(\sum_{v \in \mathrm{P}_k} p_v \mathbf{D}_k \mathbf{h}_v \mathbf{h}_v^{\mathrm{H}} \mathbf{D}_k + \mathrm{diag}\left(\sum_{v \in \overline{\mathrm{P}}_k} p_v \mathbf{D}_k \left[\mathrm{E}\left\{ |h_{v1}|^2 \right\} \ldots \mathrm{E}\left\{ |h_{va}|^2 \right\} \ldots \mathrm{E}\left\{ |h_{vA}|^2 \right\} \right]^{\mathrm{T}} \right) + \sigma^2 \mathbf{D}_k \right)^{\dagger} \mathbf{D}_k \mathbf{h}_u \,, \quad (2)$$

where P_k represents a set of users of user cluster k to which user u belongs and those of interfering users in neighboring user clusters, $\overline{\mathrm{P}}_k$ represents a set of users except P_k, and $\mathrm{E}\{.\}$ represents the expectation operation. The interference power from user $v \in \overline{\mathrm{P}}_k$ is treated as an equivalent zero-mean noise having the variance $p_v \mathbf{D}_k \left[\mathrm{E}\left\{ |h_{v1}|^2 \right\} \ldots \mathrm{E}\left\{ |h_{va}|^2 \right\} \ldots \mathrm{E}\left\{ |h_{vA}|^2 \right\} \right]^{\mathrm{T}}$ with $\mathrm{E}\left\{ |h_{va}|^2 \right\}$ being the short-term averaged (i.e., averaged over fading) propagation channel gain between user v and antenna a. Note that when $U' = 1$, Eq. (2) becomes equivalent to the weight vector of the UC approach [2]. Also note that the weight vector for downlink transmission is given by $\mathbf{w}_u$ when assuming time-division duplex transmission.

6.3 Performance Evaluation

The uplink user capacity is evaluated by computer simulation to compare UCC- and UC-based CF-mMIMO systems. Also compared is the computational complexity, which is the total number of complex multiplications required for the weight computation for all U users. For the detailed simulation procedure, refer to [3]. A antennas and U users are randomly placed in a 1×1 normalized communication area, where A=512 and $U = \{8, 16, 32, 64, 128, 256, 512\}$. In the UCC approach, the size of user cluster is set to $U'_{\mathrm{UCC}} = 8$ and a total of K=U/8 user clusters are formed. The number of antennas associated with each user cluster is set to $A'_{\mathrm{UCC}} = 16$. In the UC approach ($U'_{\mathrm{UC}} = 1$), the size of antenna cluster is set to $A'_{\mathrm{UC}} = 8$ so that the computational complexity becomes equal to the UCC approach. The user transmit power same (for all U users) is represented by the normalized transmit signal-to-noise ratio (SNR) Γ_t. This is the received SNR when the transmitter-receiver distance is equal to a normalized distance of 1. In the simulation,

Γ_t is set to $\{-60, -50, -40, -30\}$ dB, which provides the received SNR of about 58dB higher, i.e., $\{-2, 8, 18, 28\}$ dB when the transmitter-receiver distance is equal to half the average distance between two neighboring antennas. The propagation channel is assumed to be characterized by distance-dependent pathloss with pathloss exponent of 3.5, log-normally distributed shadowing loss with standard deviation of 8 dB, and Rayleigh fading. Assuming perfect knowledge of the propagation channel, the partial MU-MMSE weight is obtained using Eq. (2).

The uplink user capacity C_u [bps/Hz] of user $u(=1,\ldots,U)$ is calculated using the capacity formula $C_u = \log_2(1+\Gamma_u)$ for a set of user locations of all U users, where Γ_u represents the received signal-to-interference plus noise ratio of user u and can be derived from Eq. (1). The cumulative distribution function (CDF) of the user capacity is evaluated by randomly changing a set of user locations. Fig. 6-4 compares UC and UCC approaches in terms of the user capacity at CDF=50%. The UCC approach provides higher capacity when Γ_t = -30 dB and -40 dB (i.e., relatively high transmit power). However, when Γ_t = -50 dB and -60 dB (i.e., very low transmit power), the UCC approach provides slightly lower capacity. This is because such low transmit power makes antenna cooperation difficult for spatial multiplexing. But, even when Γ_t is set to -50 dB and -60 dB, the UCC approach provides slightly higher capacity when U gets larger.

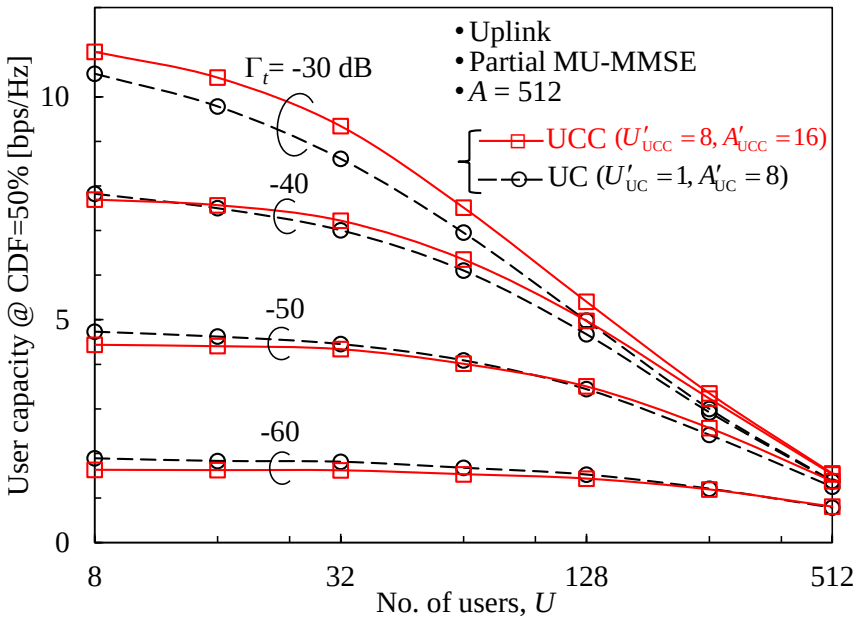

Fig. 6-4 Capacity comparison.

The relationship between the user capacity and the computational complexity is shown in Fig. 6-5 with A' as a parameter when U=512 and Γ_t = -30 dB. The computational complexity assuming the LDL^H decomposition for the inverse matrix

operation [7] is shown in Table 6-1. The UCC approach provides higher capacity than the UC approach at any level of computational complexity.

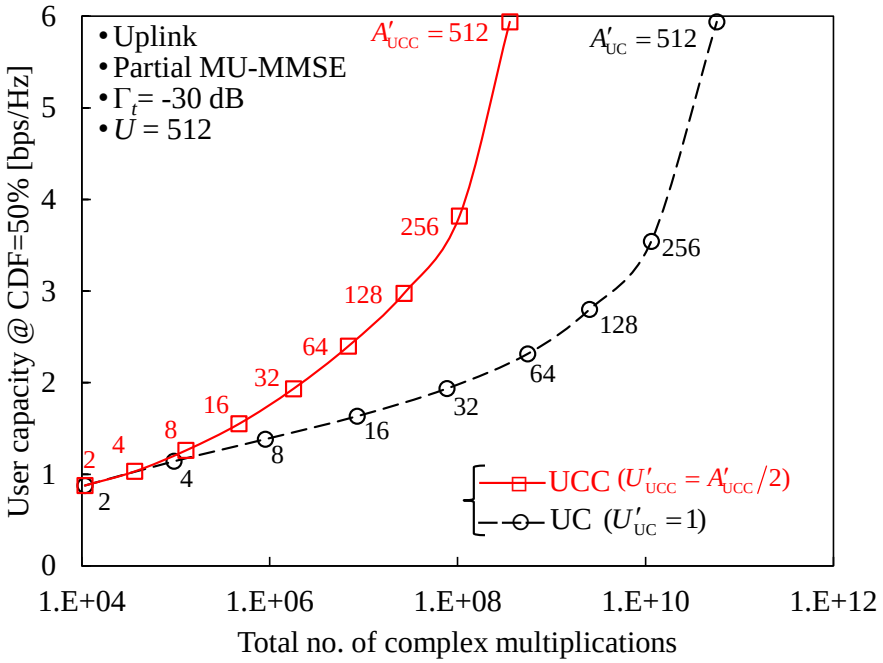

Fig. 6-5 Capacity versus complexity.

Table 6-1 Computational complexity.

Approach	No. of user clusters	The total no. of complex multiplications required for weight computation for all users
UC	$K = \frac{U}{U'_{UC}} = U$	$\left(\frac{A'^2_{UC} + A'_{UC}}{2}\left(\frac{1}{K}\sum_{k=1}^{K}\lvert P_k\rvert\right) + \frac{A'^3_{UC} - A'_{UC}}{3} + A'^2_{UC}\right)K$
UCC	$K = \frac{U}{U'_{UCC}}$	$\left(\frac{A'^2_{UCC} + A'_{UCC}}{2}\left(\frac{1}{K}\sum_{k=1}^{K}\lvert P_k\rvert\right) + \frac{A'^3_{UCC} - A'_{UCC}}{3} + A'^2_{UCC}U'_{UCC}\right)K$

6.4 Conclusion

The UCC approach utilizing partial MU-MMSE with interference suppression capability enhances CF-mMIMO systems. It should be noted that the communication area size of the CF-mMIMO system is relatively small due to the limited computing power of the CPU. It is well-known that the cellular system is the most practical approach to accommodate a large number of users over a wide communication area and that by reducing the cell size, the spectrum utilization efficiency can be improved. However, a straightforward significant reduction in cell size may not be realistic because the control data traffic related to hand-off, etc. increases significantly. The following cellular architecture combined with UCC-based CF-mMIMO could be a realistic solution [8]. Instead of reducing the cell size further than a macro-cell with a radius of several

100 meters, UCC-based CF-mMIMO is employed to form user clusters as user-centric virtual small cells within each CPU-controlled macro-cell. The size of the macro-cell can be determined by considering the computing power of each CPU.

Acknowledgements

A part of this work was conducted under "R&D for further advancement of the 5th generation mobile communication system" (JPJ000254) commissioned by the Ministry of Internal Affairs and Communications in Japan.

REFERENCE

[1] I. Kanno, K. Yamazaki, Y. Kishi, and S. Konishi, "A Survey on Research Activities for Deploying Cell Free Massive MIMO towards Beyond 5G," IEICE Trans. Commun., Vol. E105-B, No.10, pp. 1107-1116, Oct. 2022.

[2] E. Björnson and L. Sanguinetti, "Scalable Cell-Free Massive MIMO Systems," IEEE Trans. Commun., Vol. 68, Issue 7, pp. 4247 – 4261, July 2020.

[3] R. Takahashi, H. Matsuo, S. Xia, Q. Chen, and F. Adachi, "Uplink Postcoding in User cluster-Centric Cell-Free massive MIMO," IEICE Trans. Commun., Vol. E106-B, No. 9, pp. 784-757, Sep. 2023.

[4] Y. Huang, W. Lei, C. Lu, and M. Berg, "Fronthaul Functional Split of IRC-Based Beamforming for Massive MIMO Systems," Proc. IEEE VTC2019-Fall, Honolulu, Hawaii, USA, 22–25 Sep. 2019.

[5] P. Bradley, K. Bennett, and A. Demiriz, "Constrained K-means clustering", Microsoft Research Technical Report, May 2000.

[6] S. Xia, C. Ge, Q. Chen, and F. Adachi, "Cellular Structuring and Clustering for Distributed Antenna Systems," Proc. WPMC2021, Okayama, Japan, 14-16 Dec. 2021.

[7] E. Björnson, J. Hoydis, and L. Sanguinetti, "Massive MIMO Networks: Spectral, Energy, and Hardware Efficiency," Foundations and Trends in Signal Processing: Vol. 11, No. 3-4, pp. 154-655, 2017.

[8] F. Adachi, R. Takahashi, H. Matsuo, S. Xia, C. Ge, and Q. Chen, "On Design Concept of Cellular Distributed MU-MIMO for Ultra-dense RAN," Proc. IEEE APCC2022, Jeju Island, Korea, 19-21 Oct. 2022.

7 Low-Complexity User-Centric TRP Clustering Method in Downlink Cell-Free MIMO with Regularized ZF-Based Beamforming

Kenichi Higuchi, Tokyo University of Science
Hiroki Kato, Tokyo University of Science
Takanori Hara, Tokyo University of Science
Satoshi Suyama, NTT DOCOMO, INC.
Satoshi Nagata, NTT DOCOMO, INC.

***Abstract*—This article investigates a computationally-efficient method for user equipment (UE)-centric transmission reception point (TRP) clustering in downlink cell-free multi-input multi-output (MIMO) using regularized zero-forcing (RZF)-based beamforming (BF). The proposed method selects a set of TRPs used for data transmission for each UE (user-centric TRP cluster) based only on the average path gain information between UEs and TRPs. Thus, no complex calculations for a downlink BF matrix are needed for TRP clustering. Since the proposed method takes into account the BF gain and spatial interference levels for the RZF-based BF, the achievable system-level throughput can be enhanced compared to that for conventional path loss-based TRP clustering. This is achieved by utilizing the average path gain information of the target and neighboring UEs. Computer simulation results assuming a realistic partial channel state information scenario show the effectiveness of the proposed method compared to conventional methods.**

7.1 Introduction

In downlink cell-free or distributed multi-input multi-output (MIMO) [1, 2], the selection of transmission reception points (TRPs) for data transmission to each user equipment (UE), which is referred to as user-centric TRP clustering hereafter, significantly impacts the achievable system throughput. This paper investigates a computationally-efficient user-centric TRP clustering method.

User-centric TRP clustering can be categorized into two approaches. The first approach utilizes only the average path gain (or path loss) in the TRP clustering. References [1] and [3] investigated clustering methods that determine a set of TRPs in order of the highest average path gain between the target UE and each TRP. These methods achieve TRP clustering with low computational complexity since there is no need for complex calculations for a beam forming (BF) matrix. However, since the received signal and interference power levels after BF are not sufficiently considered during the TRP clustering, the achievable system-level throughput performance is not significant.

The second approach utilizes the instantaneous channel state information (CSI) in TRP clustering [4, 5]. Reference [4] investigated a TRP clustering method that maximizes the instantaneous channel gain of the target UE. This method is simple but the received signal and interference power levels after BF were not sufficiently considered. Reference [5] investigated a TRP clustering method based on the received signal power after BF and interference to other UEs, which is referred to as the signal-to-leakage-and-noise ratio (SLNR)-based method hereafter. Since the SLNR-based

method considers the BF gain during the TRP clustering, its achievable throughput performance is high. However, this method suffers from a significantly high level of computational complexity due to the complex BF matrix computations, such as channel matrix inversion. In addition, in a realistic scenario where the time interval for TRP clustering is longer than the coherence time of the wireless channel, the advantage of employing TRP clustering based on instantaneous CSI may be restricted due to the instantaneous fading variation during the TRP clustering interval.

We propose a low-complexity user-centric TRP clustering method for regularized zero-forcing (RZF)-based BF [3, 6]. The proposed method selects the TRP cluster for each UE based only on the average path gain information without the need for complex calculations for the downlink BF matrix. Since the proposed method takes into account the BF gain and spatial interference levels for the RZF-based BF, the achievable system-level throughput can be enhanced compared to that for conventional path loss-based TRP clustering. This is achieved by utilizing the average path gain information of the target UE and its neighboring UEs. Computer simulation results assuming a realistic partial CSI scenario show the effectiveness of the proposed method compared to conventional methods.

7.2 Proposed TRP Clustering Method

We consider downlink cell-free MIMO, where a set of TRPs, $\mathcal{L}$, and a set of users, $\mathcal{K}$, are distributed over the system coverage of interest. Each TRP and UE are equipped with a single antenna. All TRPs are assumed to be connected to a central processing unit (CPU), which allows joint data transmission using an arbitrary set of TRPs for each UE. For simplicity, we assume flat instantaneous fading in this paper. Let $h_{k,l}$ be the instantaneous CSI between UE $k \in \mathcal{K}$ and TRP $l \in \mathcal{L}$, where $h_{k,l} \sim CN(0, g_{k,l})$ and $g_{k,l}$ denotes the average path gain determined by the distance-dependent loss and random shadowing effect. The set of candidate TRPs for UE k clustering is denoted as $\mathcal{L}_k \subseteq \mathcal{L}$. We assume that $|\mathcal{L}_k|$ is fixed to L_{cand} for all UEs and $\mathcal{L}_k$ comprises TRPs with the L_{cand} highest average path gain between it and UE k. In this paper, a part of instantaneous CSI $h_{k,l}$ is assumed to be estimated and known at TRPs based on the uplink reference signal in a time division duplex (TDD) system. Let $S_k \subseteq \mathcal{L}_k$ be the set of TRPs that know the instantaneous CSI of UE k. Based on [3] and [5], we define S_k as the set of TRPs whose average path gain to UE k is higher than $g_{k,\max}-\Delta_{\text{CSI}}$ in decibels (dB), namely $S_k = \left\{ l \mid g_{k,l} \geq g_{k,\max} - \Delta_{\text{CSI}}, l \in \mathcal{L} \right\}$, where $g_{k,\max}$ is the maximum average path gain between UE k and all TRPs, and Δ_{CSI} is a parameter that determines the range of instantaneous CSI acquisition.

We assume RZF-based BF [3, 6] in this paper. Let $\mathcal{T}_k \subseteq \mathcal{L}_k$ be the TRP cluster for UE k. The $|\mathcal{T}_k|$-dimensional channel vector of UE k, $\mathbf{h}_k(\mathcal{T}_k)$, is represented as

$$\mathbf{h}_k(\mathcal{T}_k) = [h_{k,[\mathcal{T}_k]_1} \quad h_{k,[\mathcal{T}_k]_2} \quad \cdots \quad h_{k,[\mathcal{T}_k]_{|\mathcal{T}_k|}}]^T , \tag{1}$$

where $[\mathcal{T}_k]_l$ represents the l-th element of $\mathcal{T}_k$. Due to the partial CSI condition, $\mathbf{h}_k(\mathcal{T}_k)$ may contain unknown elements. We use the channel matrix muting method in [5] to determine the BF vector with partial CSI. The muting operation generates muted

channel vector $\tilde{\mathbf{h}}_k(\mathcal{T}_k)$ by setting the l-th element of $\mathbf{h}_k(\mathcal{T}_k)$, $h_{k,[\mathcal{T}_k]_l}$, to zero if it is not known at the TRP.

Let $\mathcal{U}_k(\mathcal{T}_k)$ be the set of UEs other than UE k for which the instantaneous CSI to TRP set $\mathcal{T}_k$ is at least partially known. Thus, $\mathcal{U}_k(\mathcal{T}_k)=\{j \mid S_j \bigcap S_k \neq \varnothing, j \neq k \in \mathcal{K}\}$. The muted channel vector between set of TRPs $\mathcal{T}_k$ and UE $j \in \mathcal{U}_k(\mathcal{T}_k)$ is denoted by $\tilde{\mathbf{h}}_j(\mathcal{T}_k)$. Let $\tilde{\mathbf{H}}_k(\mathcal{T}_k)$ be the muted channel matrix with $\tilde{\mathbf{h}}_k^T(\mathcal{T}_k)$ and $\{\tilde{\mathbf{h}}_j^T(\mathcal{T}_k)\}$ aligned in the row direction. According to the principle of RZF [6], the BF vector to UE k can be obtained from the following matrix.

$$\tilde{\mathbf{H}}_k^-(\mathcal{T}_k)=\tilde{\mathbf{H}}_k^H(\mathcal{T}_k)\left(\tilde{\mathbf{H}}_k(\mathcal{T}_k)\tilde{\mathbf{H}}_k^H(\mathcal{T}_k)+\xi\frac{N_0}{p_k}\mathbf{I}\right)^{-1}, \tag{2}$$

where p_k and N_0 are the transmission signal power allocated to UE k and the noise power, respectively. Term $\xi N_0 / p_k\mathbf{I}$ is the normalization term and ξ is a nonnegative parameter that adjusts the magnitude of the normalization term. We note that ξ includes the effect of path loss. When $\tilde{\mathbf{h}}_k^T(\mathcal{T}_k)$ is placed in the first row of $\tilde{\mathbf{H}}_k(\mathcal{T}_k)$, the BF vector to UE k corresponds to the first column vector of $\tilde{\mathbf{H}}_k^-(\mathcal{T}_k)$ after its norm is normalized to one.

When ξ is set to zero, RZF is equivalent to pure zero-forcing (ZF), which minimizes the interference power. When ξ is set sufficiently large, RZF is equivalent to maximum ratio combining (MRC), which maximizes the received signal power. The performance of RZF is between pure ZF and MRC. By selecting an appropriate ξ value for a given channel, RZF can achieve performance close to that for the minimum mean squared error (MMSE)-based BF.

We propose a computationally-efficient TRP clustering metric suitable for RZF. The proposed metric comprises a weighted sum of two metrics suitable for pure ZF and MRC. These metrics are defined as the ratio of the achievable BF gain of UE k to the spatial interference levels (leakage power) imparted to other UEs in the neighborhood when applying pure ZF and MRC-based BF.

First, we derive a metric for pure ZF, which corresponds to RZF with ξ of zero. Pure ZF based on the Moore-Penrose generalized inverse of the channel matrix can be recognized as a concatenation of ZF and MRC of the effective channels after ZF. Thus, effective channel f_k after BF of UE k assuming the candidate TRP cluster, $\mathcal{T}$, is represented as

$$f_k=\sqrt{\sum_{i=1}^{|\mathcal{T}|-|\mathcal{U}_k(\mathcal{T})|}|\tilde{\mathbf{h}}_k^T(\mathcal{T})\mathbf{z}_k^i|^2}=\sqrt{\sum_{i=1}^{|\mathcal{T}|-|\mathcal{U}_k(\mathcal{T})|}\left|\sum_{l\in\mathcal{T}}z_{k,l}^i\tilde{h}_{k,l}\right|^2}, \tag{3}$$

where $\tilde{h}_{k,l}$ is the l-th element of $\tilde{\mathbf{h}}_k(\mathcal{T})$, $\mathbf{z}_k^i$ is the i-th normalized ZF vector that is orthogonal to all channel vectors of other UE $i \in \mathcal{U}_k(\mathcal{T})$, and $z_{k,l}^i$ is the l-th element of $\mathbf{z}_k^i$. The received signal power of UE k becomes

$$|f_k|^2\ p_k=\sum_{i=1}^{|\mathcal{T}|-|\mathcal{U}_k(\mathcal{T})|}\left|\sum_{l\in\mathcal{T}}z_{k,l}^i\tilde{h}_{k,l}\right|^2 p_k\,. \tag{4}$$

The exact computation of (4) requires the calculation of the BF matrix. The proposed method applies the expectation operation to the received signal power to avoid complex

calculation of the BF matrix ($\mathbf{z}_k^i$) during the metric calculation for TRP clustering, which is given by

$$\mathrm{E}[|\ f_k\ |^2\ p_k\ ] = \sum_{i=1}^{|\mathcal{T}|-|\mathcal{U}_k(\mathcal{T})|} \sum_{l\in\mathcal{T}} \mathrm{E}\left[\left|z_{k,l}^i\right|^2 \left|\tilde{h}_{k,l}\right|^2\right] p_k = \left\{\left(|\mathcal{T}|-|\mathcal{U}_k(\mathcal{T})|\right)/|\mathcal{T}|\right\} \sum_{l\in\mathcal{T}} g_{k,l}\, p_k \ . \tag{5}$$

The sum of the estimated interference power to other UE $j \in \mathcal{U}_k(\mathcal{L}_k)$ and the expected noise power are calculated as

$$\frac{1}{|\mathcal{U}_k(\mathcal{L}_k)|} \sum_{j\in\mathcal{U}_k(\mathcal{L}_k)} \sum_{l\in\mathcal{T}\setminus S_j} g_{j,l} \left(g_{k,l} \Big/ \sum_{l\in\mathcal{T}} g_{k,l} \right) p_k + \alpha N_0 . \tag{6}$$

The second term in (6) is the product of noise power N_0 and positive coefficient parameter α. It reflects the noise power and the interference from other TRP clusters. The proposed TRP clustering metric, $\lambda_k^{\mathrm{Prop.ZF}}(\mathcal{T})$, of UE k for candidate TRP cluster $\mathcal{T}$ assuming pure ZF-based BF is obtained as

$$\lambda_k^{\mathrm{Prop.ZF}}(\mathcal{T}) = \frac{\left\{\left(|\mathcal{T}|-|\mathcal{U}_k(\mathcal{T})|\right)/|\mathcal{T}|\right\} \sum_{l\in\mathcal{T}} g_{k,l}\, p_k}{\frac{1}{|\mathcal{U}_k(\mathcal{L}_k)|} \sum_{j\in\mathcal{U}_k(\mathcal{L}_k)} \sum_{l\in\mathcal{T}\setminus S_j} g_{j,l} \left(g_{k,l} \Big/ \sum_{l\in\mathcal{T}} g_{k,l} \right) p_k + \alpha N_0} . \tag{7}$$

Based on the same idea as in the derivation of $\lambda_k^{\mathrm{Prop.ZF}}(\mathcal{T})$, the metric for MRC-based BF, $\lambda_k^{\mathrm{Prop.MRC}}(\mathcal{T})$, which corresponds to RZF with sufficiently large ξ, is obtained. The proposed metric, $\lambda_k^{\mathrm{Prop.MRC}}(\mathcal{T})$, of UE k for candidate TRP cluster $\mathcal{T}$ assuming MRC-based BF is represented as

$$\lambda_k^{\mathrm{Prop.MRC}}(\mathcal{T}) = \frac{\sum_{l\in\mathcal{T}} g_{k,l}\, p_k}{\frac{1}{|\mathcal{U}_k(\mathcal{L}_k)|} \sum_{j\in\mathcal{U}_k(\mathcal{L}_k)} \sum_{l\in\mathcal{T}} g_{j,l} \left(g_{k,l} \Big/ \sum_{l\in\mathcal{T}} g_{k,l} \right) p_k + \alpha N_0} . \tag{8}$$

Finally, by taking the weighted sum of two metrics, $\lambda_k^{\mathrm{Prop.ZF}}(\mathcal{T})$ and $\lambda_k^{\mathrm{Prop.MRC}}(\mathcal{T})$, proposed metric $\lambda_k^{\mathrm{Prop.}}(\mathcal{T})$ of UE k for candidate TRP cluster $\mathcal{T}$ for RZF-based BF is obtained as

$$\lambda_k^{\mathrm{Prop.}}(\mathcal{T}) = \beta \lambda_k^{\mathrm{Prop.ZF}}(\mathcal{T}) + (1-\beta) \lambda_k^{\mathrm{Prop.MRC}}(\mathcal{T}) , \tag{9}$$

where β is a weight coefficient that ranges from zero to one. UE k selects its clustered TRPs that maximize $\lambda_k^{\mathrm{Prop.}}(\mathcal{T})$.

7.3 Numerical Results

The user throughput for the proposed method is evaluated by computer simulation and compared to that for the conventional methods. TRPs and UEs are randomly placed in a wraparound 5 × 5-square kilometer (km^2) system coverage area according to the Poisson point process. The density of TRPs, L, of 25 and 50 per km^2 are tested. The UE density is set to 10 per km^2. The system bandwidth is 100 MHz, and the transmission signal power per UE is set to 30 dBm. The distance-dependent path loss with the decay factor of 3.76, random log-normal shadowing with a standard deviation of 8 dB, and instantaneous Rayleigh fading are simulated as the propagation channel model. The

noise power density at the UE is set to −165 dBm/Hz. Term Δ_{CSI} is set to 10 dB in the partial CSI model. In addition to the proposed method with parameter β, the path loss-based method [1, 3] and SLNR-based method [5] are evaluated as conventional methods for comparison. Parameter α included in the metrics of the proposed and SLNR-based methods is set to 10^4. Term L_{cand} is set to 15 for all TRP clustering methods. Throughput is calculated based on Shannon's capacity formula. We tested two scenarios in terms of the time interval of the TRP clustering. The first scenario is referred to as fast TRP clustering, which has an interval within a coherent interval of the channel fading. The second scenario is referred to as slow TRP clustering, which has an interval that is much longer than the channel coherence time interval.

Figs. 7-1(a) and 7-1(b) show the cumulative probability of the user throughput when pure ZF (RZF with ξ of zero) is applied to the fast and slow TRP clustering scenarios, respectively. In the path loss-based method, the maximum number of TRPs in a cluster, denoted as U, is set to 5 and 7 for L of 25 and 50, respectively. Fig. 7-1(a) shows that the path loss-based method is significantly degraded at a low cumulative probability compared to the other methods. This is mainly due to the fact that the path loss-based method does not consider the degrees of freedom of the MIMO channel and the received signal power after BF. The proposed method achieves throughput close to that of the SLNR-based method while avoiding complex calculation of the BF matrix for TRP clustering. This is because the proposed method performs TRP clustering based on the estimated power gain at BF considering the degrees of freedom of the MIMO channel and the interference to other UEs in the neighborhood. Fig. 7-1(b) shows that the proposed method outperforms the two conventional methods in the slow TRP clustering scenario. In the SLNR-based method, which is based on the instantaneous channel condition, the optimal TRP clustering changes with instantaneous channel fading. Hence, the SLNR-based method tends to be degraded by the instantaneous fading variation after TRP clustering in the slow TRP clustering scenario. Since the proposed method is based on the average channel conditions, the proposed method is particularly effective in a realistic slow TRP clustering scenario.

Figs. 7-2(a) and 7-2(b) show the average and 5%-outage user throughput as a function of ξ, respectively. The slow TRP clustering scenario is assumed. The proposed method and conventional path loss-based method are compared. For each TRP clustering method, the average number of TRPs used per UE, N_{TRP}, is fixed at four by adjusting the maximum number of TRPs in the cluster. In the proposed method, β of 0.5, 1.0, and 0.0 are tested. Fig. 7-2(a) shows that the proposed method outperforms the path loss-based method regardless of ξ and L. The β value achieving the highest throughput varies depending on ξ. For instance, at ξ of 10^3 where the effect of RZF is greatest under the assumed channel conditions, the proposed method with β = 0.5 achieves the highest performance. Fig. 7-2(b) shows that the proposed method with β = 0.5 is most effective also in terms of the 5%-outage user throughput at ξ of 10^3.

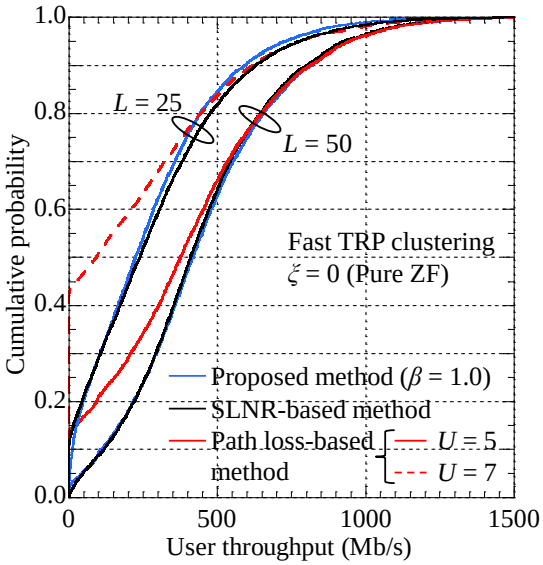

(a) Fast TRP clustering.

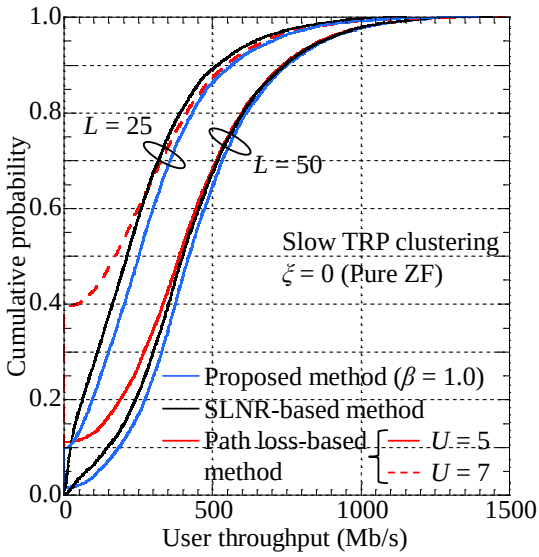

(b) Slow TRP clustering.

Fig. 7-1 User throughput distribution at ZF-based BF.

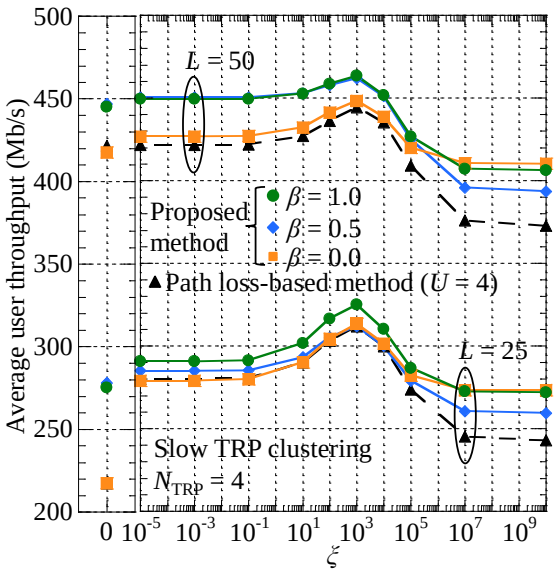

(a) Average user throughput.

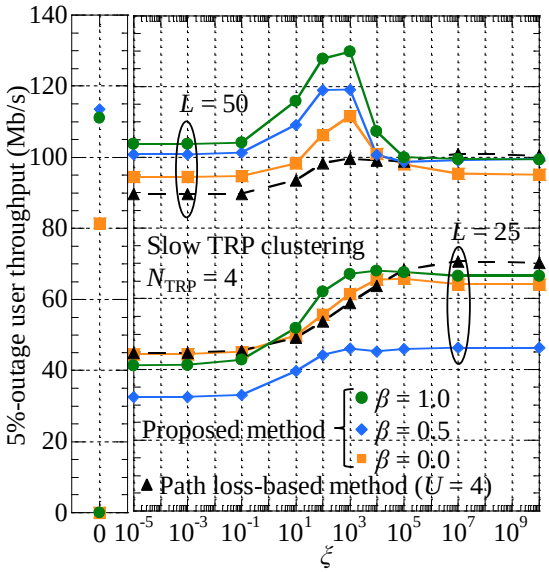

(b) 5%-outage user throughput.

Fig. 7-2 User throughput distribution as a function of ξ.

7.4 Conclusion

We investigated downlink cell-free MIMO in a partial CSI scenario and proposed a low-complexity user-centric TRP clustering method with RZF-based BF. The proposed method selects the TRP cluster for each UE based only on the average path gain information between UEs and TRPs. The proposed method does not require complex calculation of the BF matrix. The proposed method considers the BF gain and spatial

interference levels, which is different from the conventional path loss-based method. Computer simulation results assuming a realistic partial CSI scenario show the effectiveness of the proposed method in terms of the achievable system-level throughput compared to the conventional path loss-based and SLNR-based methods.

REFERENCE

[1] E. Björson and L. Sanguinetti, "Scalable cell-free massive MIMO systems," IEEE Trans. Commun., vol. 68, no. 7, pp. 4247-4261, Jul. 2020.

[2] I. Kanno, K. Yamazaki, Y. Kishi, and S. Konishi, "A survey on research activities for deploying cell free massive MIMO towards beyond 5G," IEICE Trans. Commun., vol. E105-B, no. 10, pp. 1107-1116, Oct. 2022.

[3] M. Mojahedian and A. Lozano, "Subset regularized zero-forcing precoders for cell-free C-RANs," in Proc. IEEE EUSIPCO2021, Ireland, Aug. 2021.

[4] S. Buzzi, C. D'Andrea, A. Zappone, and C. D'Elia, "User-centric 5G cellular networks: Resource allocation and comparison with the cell-free massive MIMO approach," IEEE Trans. Commun., vol. 19, no. 2, pp. 1250-1264, Feb. 2020.

[5] Y. Oshima, A. Benjebbour, and K. Higuchi, "A novel adaptive interference admission control method for layered partially non-orthogonal block diagonalization for base station cooperative MIMO," IEICE Trans. Commun., vol. E97-B, no. 1, pp. 155-163, Jan. 2014.

[6] C. B. Peel, B. M. Hochwald, A. L. Swindlehurst, "A vector-perturbation technique for near-capacity multiantenna multiuser communication-part I: Channel inversion and regularization," IEEE Trans. Commun., vol. 53, no. 1, pp. 195-202, Jan. 2005.

[7] H. Q. Ngo, *et al.*, "Cell-free massive MIMO versus small cells," IEEE Trans. Wireless Commun., vol. 16, no. 3, pp. 1834-1850, Mar. 2017.

8 Toward Practical Cell-Free MIMO Network

Koji Ishibashi, The University of Electro-Communications

Abstract— **As a promising enabler for beyond 5G and 6G, cell-free multiple-input multiple-output (MIMO) networks have been actively discussed. This article introduces practical bottlenecks of cell-free MIMO networks and briefly overviews related work.**

8.1 Introduction

Cell-free MIMO is a promising technique for beyond 5G and 6G, offering uniform quality of communications to user equipment (UE) through full or partial cooperation among access points (APs) controlled by a central processing unit (CPU). To clarify the concept of cell-free networks, Fig. 8-1 illustrates four different network architectures: (a) traditional cellular network including small-cell networks, (b) cellular network with distributed antennas, so-called distributed antenna system (DAS), (c) cell-free network with a single CPU, and (d) cell-free network with multiple CPUs. In traditional cellular networks, UEs near cell-edges would suffer from interference from neighboring cells besides the weak received power of the desired signals due to the path-loss. Also, if the number of antennas co-located at each base station (BS) increases, the spatial correlation would limit the resulting capacity.

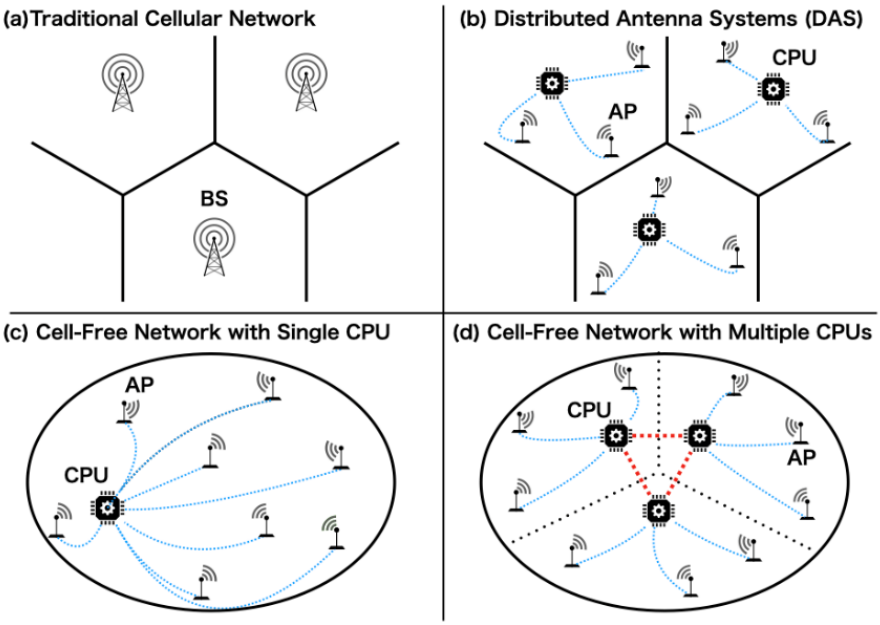

Fig. 8-1 Illustration of (a) traditional cellular network, (b) cellular network with distributed antennas, (c) cell-free network with a single CPU, and (d) cell-free network with multiple CPUs (blue dashed curves indicate fronthaul links and red backhaul).

Meanwhile, if the distributed antennas are employed, this capacity limitation can be resolved while the interference limited regime at the cell edge still holds. To overcome

this cell edge problem, the system has to treat the interference not stochastically but deterministically. Hence, cell-free network where all the antennas are jointly controlled by a single CPU emerged [1]. Note that, mathematically, cell-free network is equivalent to a distributed antenna system without the other cells or small-cell configuration, namely highly dense BS placement with a single antenna, with full cooperation among BSs [2]. As obvious, this configuration does not have the *cell-boundary*, so that interference among different streams can be completely eliminated through spatial precoding or combining, resulting in the uniform service quality over the network. However, this centralized processing architecture leads to the remarkably high (or almost impossibly high) load at the CPU. Therefore, exchanged signal reduction based on clustering has been actively discussed [3]. Considering latency and cost for fronthaul links between APs and CPU, the assumption of the single CPU is still not viable. Recently, cell-free network with multiple CPUs has been studied [4]. Note that, this architecture is mathematically and conceptually identical to a cellular network with distributed antennas with full cooperation among BSs, dubbed virtual MIMO [5] or network MIMO [6]. Although cell-free MIMO networks (or their variants) have been discussed for an extended period, due to its demanding implementation cost such as phase/time synchronization among APs and fronthaul/backhaul deployment between APs and the CPU, the integration of these technologies into standardization or introduction to the market has not much progressed. This article summarizes fundamental practical difficulties of cell-free MIMO networks and explores related efforts aimed at addressing them.

8.2 Fronthaul and Backhaul Limitations

Every AP is connected to a CPU via a dedicated optical fiber cable called fronthaul. Since the transmission rate of this fronthaul has to transmit complex signals at the speed of the (Nyquist) symbol period especially in case of uplink transmission. Considering the specifications of the current standard interface called Common Public Radio Interface (CPRI), this requirement is definitely challenging, and the resulting cost to deploy the cell-free network is the main bottleneck for practical implementation. A judicious option to alleviate this requirement is to use low-resolution analog-to-digital converters (ADCs) [7][8]. In [7], the uplink signal detection in cell-free networks subject to limited fronthaul link capacity and highly correlated channel condition has been discussed. In [8], joint channel and data estimation (JCDE) based on Bayesian inference was proposed for the uplink transmission of cell-free networks with limited fronthaul link capacity. Another approach is a radio stripe connecting APs in daisy chain; sequentially connected APs share the same fronthaul and power supply [9], leading to low-cost implementation of cell-free network. Using local processing at each AP, the radio stripe can reduce the total

amount of data transmitted over fronthaul. This architecture however can be deployed to specific environments such as stadiums and train stations, and larger delay is unavoidable through the daisy chain network than a star topology as illustrated in Fig 8-1(c).

Cell-free MIMO network with multiple CPUs offers increased deployment flexibility, so that it can be considered as the most promising and practical architecture to cover a large service area. However, this architecture necessitates a high-speed backhaul, as CPUs must exchange received signals, channel state information (CSI), and signals of various upper layers. This information exchange poses challenges, even when employing user-centric clustering to restrict the volume of such information. In [10], the joint design of beamforming and user-centric clustering has been investigated under the limitation of backhaul capacity, revealing the actual gain achieved through multiple CPU cooperation.

8.3 Network-Assisted Full Duplex

Most existing contributions assume time division duplex (TDD) with the assumption of channel duality between uplink and downlink. At the beginning of coherent transmission block, channel estimation is performed via uplink pilot transmission. Then, the block is divided into uplink and downlink as illustrated on the left of Fig. 8-2. However, the overhead associated with separating uplink and downlink in TDD imposes inevitable delay, leading to inferior overall system performance and difficulty to meet all the users' demands. Therefore, the optimal duplex design for cell-free networks is actively discussed.

One possible solution to overcome this problem is to implement in-band full-duplex technology at each AP. However, this technology requires remarkably complex signal processing, making it less preferable due to a large number of required APs in the network. Without changing the hardware of APs, network-assisted full-duplex (NAFD) has been proposed [11][12][13][14][15], where each AP is assigned to either uplink or downlink to enable full-duplex transmission through the whole network as illustrated on the right of Fig. 8-2. In [12][13], optimal AP configuration and the corresponding beamforming have been derived using convex optimization techniques, and it is shown that optimized NAFD significantly outperforms conventional TDD in terms of the sum spectral efficiency and user fairness. Since these papers assumed the perfect CSI in optimization, the AP configuration using large scale fading has been further investigated [14][15]. In [14], practical user-centric clustering and downlink power control have been proposed, where APs in a cluster for each UE must have the same transmission direction, namely either uplink or downlink, and clusters with the same transmission direction can share APs. NAFD-based cell-free network with this practical clustering remarkably

improves the sum spectral efficiency when the fronthaul capacity is limited.

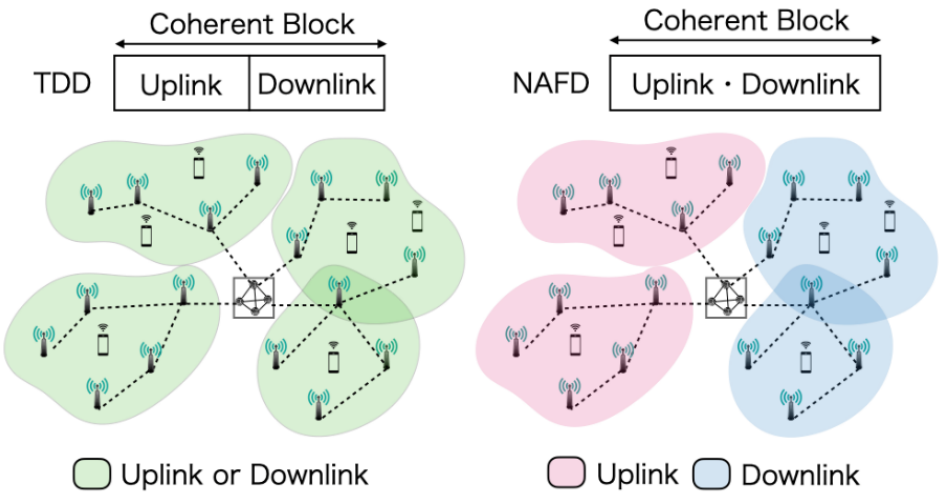

Fig. 8-2 Cell-free networks based on (left) time division duplex (TDD) and (right) network assisted full-duplex (NAFD).

8.4 Other Necessary Technologies

In this section, remaining other problems are overviewed. To initiate communications, it is necessary to transmit a request without a grant from a BS in current cellular networks. In [16], grant-free access for cell-free networks has been studied. Using bilinear framework, this approach exhibits the superior performance comparable to grant-based transmission, enabling the low latency initialization.

Moreover, considering diverse use cases in beyond 5G and 6G, UEs may have completely different communications capability and requirements, for example the number of antennas and the number of data streams. In [17], cell-free network with heterogeneous assumption, in which UEs have arbitrary number of antennas and data streams, has been studied. The proposed tensor-decomposition based beamforming outperforms popular conventional beamforming with lower or similar complexity.

Finally, to realize the coherent transmission over APs, all the APs must synchronize in time and phase, which is not viable, especially when the size of the network becomes large. Recently, mixed coherent and non-coherent transmission has been proposed [18] where only APs controlled by the same CPU are synchronized. Although this approach mitigates the synchronization requirement, the resulting system is mathematically same as a DAS with flexible cells. Considering a non-negligible leap to deploy distributed antennas, a repeater-assisted MIMO system has been proposed as an interim technology [19], enabling significant throughput performance comparable to cell-free MIMO networks.

8.5 Conclusion

This article introduces the practical difficulties of cell-free MIMO networks and provides a brief overview of papers that address these challenges. While some remarkable contributions have successfully addressed fundamental issues, there still exists a significant gap between theory and practice. This underscores the need for additional research and experiments to bridge this divide.

Acknowledgements

The author extends sincere thanks to his collaborators including current and past members of his laboratory for their dedication. Moreover, the author would like to express his sincere gratitude to Prof. Takumi Takahashi and Dr. Hiroki Iimori for their valuable comments.

REFERENCES

[1] H. Q. Ngo, A. Ashikhmin, H. Yang, E. G. Larsson and T. L. Marzetta, "Cell-Free Massive MIMO: Uniformly great service for everyone," *2015 IEEE 16th Intl. Workshop on Signal Process. Adv. in Wireless Commun.* (SPAWC), Stockholm, Sweden, pp. 201-205, 2015.

[2] J. Hoydis, M. Kobayashi and M. Debbah, "Green Small-Cell Networks," *IEEE Veh. Technol. Mag.*, vol. 6, no. 1, pp. 37-43, March 2011.

[3] E. Björnson and L. Sanguinetti, "Scalable Cell-Free Massive MIMO Systems," *IEEE Trans. Commun.*, vol. 68, no. 7, pp. 4247-4261, July 2020.

[4] Z. H. Shaik, E. Björnson and E. G. Larsson, "MMSE-Optimal Sequential Processing for Cell-Free Massive MIMO With Radio Stripes," *IEEE Trans. Commun.*, vol. 69, no. 11, pp. 7775-7789, Nov. 2021.

[5] X. Hong, Y. Jie, C. -X. Wang, J. Shi and X. Ge, "Energy-Spectral Efficiency Trade-Off in Virtual MIMO Cellular Systems," *IEEE J. Sel. Areas Commun.*, vol. 31, no. 10, pp. 2128-2140, October 2013.

[6] M. K. Karakayali, G. J. Foschini and R. A. Valenzuela, "Network coordination for spectrally efficient communications in cellular systems," *IEEE Wireless Commun.*, vol. 13, no. 4, pp. 56-61, Aug. 2006.

[7] K. Ando, H. Iimori, T. Takahashi, K. Ishibashi, and G. T. F. de Abreu, "Uplink Signal Detection for Scalable Cell-Free Massive MIMO Systems With Robustness to Rate-Limited Fronthaul," *IEEE Access*, vol. 9, pp. 102770 – 102782, July 2021.

[8] T. Takahashi, H. Iimori, K. Ando, K. Ishibashi, S. Ibi, and G. T. F. de Abreu, "Bayesian Receiver Design via Bilinear Inference for Cell-Free Massive MIMO with Low-Resolution ADCs," *IEEE Trans. Wireless Commun.*, vol. 22, no. 7, pp. 4756-4772, July 2023.

[9] Z. H. Shaik, E. Björnson and E. G. Larsson, "MMSE-Optimal Sequential Processing

for Cell-Free Massive MIMO With Radio Stripes," *IEEE Trans. Commun.*, vol. 69, no. 11, pp. 7775-7789, Nov. 2021.
[10] M. Ito, S. Fukue, K. Ando, I. Kanno, K. Yamazaki, and K. Ishibashi, “Clustering and Beamforming for User-Centric Cell-Free Massive MIMO With Backhaul Capacity Limitation,” *IEEE Access*, vol. 12, pp. 382-395, 2024.
[11] D. Wang, M. Wang, P. Zhu, J. Li, J. Wang and X. You, "Performance of Network-Assisted Full-Duplex for Cell-Free Massive MIMO," *IEEE Trans. Commun.*, vol. 68, no. 3, pp. 1464-1478, March 2020.
[12] S. Fukue, H. Iimori, G. T. F. De Abreu and K. Ishibashi, “Joint Access Configuration and Beamforming for Cell-Free Massive MIMO Systems With Dynamic TDD,” *IEEE Access*, vol. 10, pp. 40130-40149, Apr. 2022.
[13] S. Fukue, G. T. Freitas de Abreu and K. Ishibashi, "Network-Assisted Full-Duplex Millimeter-Wave Cell-Free Massive MIMO with Localization-Aided Inter-User Channel Estimation," *2023 Intl. Conf. on Inf. Networking (ICOIN)*, Bangkok, Thailand, pp. 13-18, 2023.
[14] K. Okui, K. Ando, G. Abreu and K. Ishibashi, "Scalable Network-Assisted Full-Duplex Cell-Free Massive MIMO With Limited Fronthaul Capacity," *IEEE VTC2023-Fall*, Hong Kong, pp. 1-5, 2023.
[15] H. Iimori, J. Huschke, and J. Vieira, " Radio Unit Configuration for Dynamic Time Division Duplex in Distributed MIMO Systems," *IEEE GLOBECOM*, Kuala Lumpur, Malaysia, pp. 2543-2548, 2023.
[16] H. Iimori, T. Takahashi, K. Ishibashi, G. T. F. de Abreu, and W. Yu, “Grant-Free Access via Bilinear Inference for Cell-Free MIMO With Low-Coherence Pilots,” *IEEE Trans. Wireless Commun.*, vol. 20, no. 11, pp. 7694-7710, Nov. 2021.
[17] K. Ando, H. Iimori, G. T. F. de Abreu, and K. Ishibashi, “User-Heterogeneous Cell-Free Massive MIMO Downlink and Uplink Beamforming via Tensor Decomposition,” *IEEE Open J. Commun. Soc.*, vol. 3, pp. 740-758, Apr. 2022.
[18] R. P. Antonioli, I. M. Braga, G. Fodor, Y. C. B. Silva and W. C. Freitas, "Mixed Coherent and Non-Coherent Transmission for Multi-CPU Cell-Free Systems," *IEEE ICC 2023*, Rome, Italy, 2023, pp. 1068-1073.
[19] H. Iimori, E. Kurihara, T. Yoshida, J. Vieira, and S. Malomsoky, “Amplification Strategy in Repeater-Assisted MIMO Systems via Minorization Maximization,” *IEEE GLOBECOM*, Kuala Lumpur, Malaysia, Dec. 4–8, 2023